AN ABSTRACT OF THE THESIS OF

Alan Lee Flint for the degree of Doctor of Philosophy

in Soil Science presented on May 5, 1986

Title: Measured and Modeled Energy Balance Parameters to Evaluate the Environmental Conditions of Reforestation

Abstract Approved:

Stuart Childs

In order to develop three models for use in quantifying the environmental conditions of reforestation, extensive measurements required for energy balance calculations were taken for a reforestation site in southwest Oregon. The models are used to decrease the number of measurements required to properly evaluate the potential for heat or moisture stress at a specific reforestation site.

The first model, a modification of the Priestley-Taylor evaporation equation, is calibrated to allow prediction of actual evaporation from net radiation and soil heat flux under nonsaturated, soil water limited conditions. By combining Bowen ratio measurements of evaporation and soil water content, an equation was developed to calculate a modified Priestley-Taylor coefficient, α', as a function of soil water content. When the soil is near field capacity α' is ≈ 0.85. Under drier soil

conditions, the decrease in α is well described by an exponential equation. The soil water content did not become limiting to evapotranspiration until 60 percent of the available water was used.

The second model uses the inverse solution to the soil heat flow equation to determine soil thermal conductivity for layered, heterogeneous soils. The results of the model indicate that soil thermal properties could be adequately modeled by separating the soil into four physical layers to account for the variability in soil water content, bulk density and rock fragment content. The four layer soil model could predict temperatures within 0.3°C and soil heat flux within 0.006 $MJ/m^2/day$.

The third model predicts solar radiation. The model incorporates thorough treatment of all components of radiation, (Rayleigh scatter, aerosol scatter, multiple reflected, ground reflected and direct beam radiation) yet only requires the basic site measurements of slope, aspect, latitude, longitude, elevation, and ground albedo. These data are combined with a simple estimate of turbidity (either from a local weather station or literature values) and literature values for atmospheric content of ozone and water vapor to provide a good estimate of potential solar radiation. The model also considers the anisotropic distribution of diffuse radiation and the strong influence that blocking ridges have on total diffuse radiation as well as direct beam. The model was tested using data collected from six sites with different atmospheric conditions and topographic settings.

MEASURED AND MODELED ENERGY BALANCE PARAMETERS TO EVALUATE THE ENVIRONMENTAL CONDITIONS OF REFORESTATION

by

Alan L. Flint

A THESIS

submitted to

Oregon State University

in partial fulfillment of

the requirements for the

degree of

Doctor of Philosophy

Completed May 5, 1986

Commencement June 1986

APPROVED:

Redacted for Privacy

Professor of Soil Science in charge of major

Redacted for Privacy

Head of Department of Soil Science

Redacted for Privacy

Dean of Graduate School

Date thesis is presented: May 5, 1986

ACKNOWLEDGEMENTS

I would like to acknowledge the support of the Forestry Intensified Research Program, the USDA Forest Service and the USDI Bureau of Land Management. Their far sighted goals and commitment to reforestation in southwest Oregon make this research project possible.

I owe many thanks to enumerable people who have helped with this project. For reviewing the manuscripts thanks go to Stuart Childs, Mike Schuyler, Jim Vomicil, Jim Boyle, and Larry Boersma. The field work was a cooperative effort with thanks going to Stuart, Lorrie, Theresa, and Dick. I also want to thank Jayne and the rest of the office staff for allowing the freedom to work.

There were times when I was unsure that it was worth the struggle. During those time there is a tremendous need for others to yield from the educational process to give us encouragement. I want to thank Stuart Childs for recognizing those times else I fear I would not be here. Without his support and guidance I would not know the value and true meaning of the scientific method.

I would like to thank my parents for their support and love, their belief in me has helped. I would like to thank my in-laws for their support, particularly Bob and Mary Jo, who have shared their insights into academic pursuits. I have an unpayable debt to my wife, Lorrie, for her steadfast support and encouragement during the best of times but particularly during the worst of times. I am proud to be her friend. I want to thank my girls, Melissa and Megan, for giving me a reason to do the best I can.

I have special thanks to give to Craig for his concern, friendship, and personal interest. I would also like to thank him for our long and fruitful discussions on the history and principles of soil physics, a part of education we to often ignore.

I also want to thank my friend Milda for seeing me through these last days, she has been a good friend.

I want to thank the Lord for his silent support.

In the end I thank everyone for allowing me the opportunity to pursue a dream.

TABLE OF CONTENTS

LIST OF FIGURES

LIST OF FIGURES (Continued)

LIST OF TABLES

LIST OF TABLES (Continued)

MEASURED AND MODELED ENERGY BALANCE PARAMETERS TO EVALUATE THE ENVIRONMENTAL CONDITIONS OF REFORESTATION

INTRODUCTION

Reforestation failures in southwest Oregon have been a significant problem for many years. Our understanding of the environmental conditions which have contributed to these failures has been limited by lack of intensive, long term measurements. Without clear evidence regarding the cause of reforestation failure managers have been forced to use a "case study" approach to test various practical techniques to ameliorate harsh microclimate. This trial and error approach is expensive and provides inconclusive results because the environmental conditions which cause reforestation failures do not occur every year. Continuous monitoring may be necessary to gather the environmental data which will provide insight into those extremes in environment which cause seedling mortality. Although the need for intensive, long term measurements is evident, it will not be met in the near future.

Models provide an alternative to collection of extensive long term data. They can be used to quantify environmental parameters, such as extremes in soil temperatures, under a large variety of conditions (e. g. thick organic layers, rock layers, shallow soils, moisture limited conditions). Models are also used to test the sensitivity of environmental systems to changes in various

parameters, such as change in the radiation environment, soil water content, vegetation cover and air temperature. Models should not, however, be used to completely replace measurements.

Although use of extensive measurements to evaluate reforestation sites is of value, the measurement approach has inherent problems. The environmental conditions, measured for a potential reforestation site, will change after harvesting. Regeneration of forest species and encroachment by competing vegetation will cause changes in soil water distribution and use for several years. The timing of soil water loss will not only be affected by the change in vegetative cover but perhaps more significantly by changes in the near-surface radiation microclimate.

The best solution is probably the combination of extensive measurements and modeling. The measurements made during this study were intended to characterize forest clearcuts of 1 to 20 Ha in size. The models designed to be applied on the same scale can be used for specific microsite investigations. The models should account for the specific conditions of the site but allow for the influence of nearby soil and vegetation conditions as they influence the local microclimate. A combined measurements and modeling approach should account for the variability of environmental conditions due to variability in soil properties and vegetative cover.

The intent of this thesis is to develop information which allows the incorporation of models to help evaluate the

environmental conditions that will exist for a site during reforestation. The focus of the measurements and modeling was characterization of the energy balance:

$$Q^* - G + S + \lambda E = 0 \qquad (1)$$

where Q^* is net radiation, G is soil heat flux, S is sensible heat flux and λE is the latent heat flux (λ is the latent heat of vaporization of water and E is the quantity of water evaporated or condensed on the surface). The intent is not to solve the energy balance for the component parts but to use the energy balance framework to analyze the most critical parts and concentrate measurement efforts on those parameters which cannot be adequately modeled. The models will then help to focus the need for long term measurements of environmental parameters by identifying those measurements which are most critical to reforestation microclimate. The investigation of the environmental parameters of soil heat flow and evapotranspiration should yield, at least in part, a solution to the problem of seedling survival.

Solar Radiation

The major component of net radiation (Q^*) is solar radiation. Adequate methods are available for long term radiation measurement but these measurements are too expensive to be routinely made on a large number of sites. Of the radiation models available, none are

appropriate for sloping sites in mountainous terrain. Many models predict radiation in the absence of an atmosphere and therefore can only be used in relative terms. Other models do not account for the proper distribution of diffuse radiation or ground reflected radiation which may be a significant part of the total radiation when surrounding topography blocks direct beam radiation as well as a significant portion of the diffuse radiation. Another important consideration in modeling radiation is the view the soil surface has of the surrounding topography. In early spring, a bare soil surface facing south may receive a significant amount of reflected radiation from the opposite, north facing slope if it has a high albedo due to a longer lasting snow cover. Therefore an objective of this research is to develop a model of solar radiation for mountainous terrain which accounts for effects of surrounding topography. It would be advantageous if the model could be applied with only a small input data requirement.

Latent Heat Flux

Perhaps the most important site evaluation is that of soil water storage and evaporative demand. The model used to estimate seasonal evapotranspiration is based on the Priestley-Taylor equation. This model was chosen because of the small number of needed environmental measurements: air temperature, net radiation and soil heat flux. Also, the Priestley-Taylor model can be modified to give actual evapotranspiration using soil water

information. The application of the model incorporates a function of soil water content since it is soil water that generally limits evaporation late in the season when soil water allocation and use are most critical to seedling survival.

Soil Heat Flux

Another critical component to seedling survival is soil temperature. It is difficult and perhaps impractical to separate soil water use and soil temperature. It is generally the lack of soil water during periods of high radiation loads which contribute to high soil temperatures and seedling mortality. We applied the inverse solution technique to the soil heat flow equation to estimate the thermal conductivity of a heterogeneous forest soil. The resulting conductivity values were used with a numerical method to predict soil temperatures and soil heat flux.

Summary

The three chapters in the thesis cover the energy balance parameters of net radiation, soil heat flux, sensible heat flux and latent heat flux. Sensible heat flux is not treated separately but is only used in the Bowen ratio method to calculate latent heat flux. The resultant latent heat flux model then eliminates the need to measure sensible heat flux. The three models, latent heat flux, soil heat flux and solar radiation, can be used with

measurements of air temperature and soil surface temperature to predict soil heat flow, soil profile temperatures and evaporation from horizontal or sloping surfaces in mountainous terrain. An equally useful application of the models is to simplify the requirement for extensive measurements for adequate description of a reforestation site. The application of models in conjunction with measurements should provide a technique to better test hypotheses regarding the influence of soil and vegetative conditions on heat and moisture stress.

1. Use of the Priestley-Taylor Evaporation Equation for Soil Water Limited Conditions

Alan L. Flint and Stuart W. Childs

Department of Soil Science

Oregon State University

Use of the Priestley-Taylor Evaporation Equation for Soil Water Limited Conditions

Alan L. Flint and Stuart W. Childs[2]

ABSTRACT

Extensive measurements required for energy balance calculations were taken for a reforestation site in southwest Oregon. The Bowen ratio method was used to calculate latent heat flux over the growing season. These values were used to modify the

---

[1]Oregon Agric. Exp. Stn. Technical paper no.____. Contribution of the Dept. of Soil Science, Oregon State Univ., Corvallis, OR. This work was supported as part of the Forestry Intensified Research Program (PNW-80-85), a cooperative project of Oregon State University, the USDA Forest Service, and the USDI Bureau of Land Management.

[2]Graduate Research Assistant and Assistant Professor, Respectively, Dept. of Soil Science, Oregon State University, Corvallis, OR 97331.

Priestley-Taylor coefficient, α, for conditions where actual evapotranspiration is less than potential. The Priestley-Taylor coefficient is approximately equal to 0.8 for the partially vegetated surface when the soil is near field capacity. There is a decrease in the value of α associated with a decrease in soil water content which is adequately described by a simple exponential equation. The soil water content did not become limiting to evapotranspiration until 60% of the available soil water was used.

A technique is proposed to eliminate the requirement for measured net radiation and soil heat flux in the Priestley-Taylor equation. Use of this technique requires one time measurements for the site radiation balance and use of solar radiation and soil heat flux models. The resulting form of the Priestley-Taylor equation would be of value for sites where few measurements are available.

INTRODUCTION

A major limitation of many reforestation sites is lack of water during the growing season. In areas with xeric climates, this is often combined with high temperatures which increase the potential for plant stress. Therefore, any assessment of harshness of reforestation sites requires information regarding both water supply and environmental demand. The measurement and evaluation of a surface energy budget is a useful analytical approach because components of both the heat and water environments are included. This approach does, however, require detailed, site specific measurements.

A number of simplifications of the energy budget techniques have been used in order to decrease the quantity and intensity of measurements required. The Penman equation (Penman, 1948) is commonly used in situations where detailed environmental data are available. The simplifications used to model the aerodynamic parts of the equation make the equation useful only for calculation of potential evapotranspiration. Furthermore, the equation requires calibration. The Penman-Monteith combination equation (Monteith, 1966) allows calculation of actual evapotranspiration but requires detailed knowledge about the resistance to water flow at the evaporating surface. Priestley and Taylor (1972) suggested a modification of the Penman equation for potential evapotranspiration which requires less extensive measurements. It

has been demonstrated to give good results (e.g. De Bruin and Holtslag, 1982). The Priestley-Taylor formulation is:

$$\lambda E_p = \alpha \cdot \frac{s}{s+\gamma} \cdot (Q^* - G) \qquad (1.1)$$

where λE_p is the potential latent heat flux, α is a model coefficient, s is the slope of the saturation vapor density curve, γ is the pyschrometric constant, Q^* is net radiation and G is soil heat flux. In this formulation the aerodynamic term is modeled as $(\alpha-1)\cdot[s/(s+\gamma)]\cdot(Q^*-G)$. This simplification is successful because the radiation term generally dominates the aerodynamic term (Stewart, 1983).

The coefficient α was first calculated by Priestley and Taylor (1972) for daily application and is considered to be 1.26 for a freely evaporating surface (Priestley and Taylor, 1972; Stewart and Rouse, 1977). For practical applications, the Priestley-Taylor coefficient, α, depends on surface vegetation conditions. Literature values of α range from 1.57 for conditions of strong advection of sensible heat to 0.80 for a thinned Douglas-fir forest (Table 1.1).

Although the value of α under moist surface conditions ($\alpha>1$) may be a function of wind speed and aerodynamic resistance, under dryer conditions ($\alpha<1$) it is more a function of surface resistance (De Bruin, 1983). Under dry conditions, actual evapotranspiration is usually lower than potential and depends on soil water status, properties of the vegetative surface and environmental demand

Table 1.1. Range of measured values for the Priestley-Taylor coefficient, α, under a variety of surface conditions.

α	Surface conditions	Reference
1.57	High advective conditions	Jury and Tanner, 1975
1.29	Grass (soil at field capacity)	Mukammal and Neumann, 1977
1.27	Irrigated ryegrass	Davies and Allen, 1972
1.26	Saturated surface	Priestley and Taylor, 1972
1.26	Open water surface	Priestley and Taylor, 1972
1.26	Wet meadow	Stewart and Rouse, 1977
1.18	Wet Douglas-fir forest	McNaughton and Black, 1973
1.12	Short grass	De Bruin and Holtslag, 1982
1.05	Douglas-fir forest	McNaughton and Black, 1973
1.04	Bare soil surface	Barton, 1979
0.84	Douglas-fir forest Unthinned	Black, 1979
0.80	Douglas-fir forest Thinned	Black, 1979
0.73	Douglas-fir forest (Daytime)	Giles et al, 1984
0.72	Spruce forest (Daytime)	Shuttleworth and Calder, 1979

(Black, 1979; De Bruin, 1983; Denmead and Shaw, 1962; Priestley and Taylor, 1972; Tanner and Jury, 1975). Methods involving calculation of surface resistance have generally been based on the Penman-Monteith equation. Use of the Priestley-Taylor equation for calculation of actual evapotranspiration has involved empirical relationships to soil water content. Use of the Priestley-Taylor equation to calculate actual latent heat flux can be accomplished by redefining α as a function of soil water content (Mukammal and Neumann, 1977, Davies and Allen, 1972, Barton, 1979). Another approach common in the literature is to define a soil water content below which evapotranspiration is limited and the Priestley-Taylor equation is in error. This soil water content varies greatly with soil type, vegetation and environmental demand but covers a much smaller range when expressed as a percentage of total available soil water (Table 2.1). For vegetated surface, 50 to 80 percent of the available soil water can be extracted at the potential rate. For a bare soil, evaporation was limited when 40 percent of the available water was removed. This result is not unexpected (Tanner and Jury, 1976).

OBJECTIVE

The objective of this research was to calibrate the modified Priestley-Taylor equation for soil water limited conditions. This is done by redefining the coefficient, α to be a function of soil water content (α'). Since soil water status changes with depth, we also examined the relationship between the modified coefficient,

Table 1.2. Percentage reduction in available water (θ_c) before soil water content becomes limiting to evapotranspiration.

θ_c	Surface conditions	Reference
82	Douglas-fir forest (Low Demand)	Black and Spittlehouse, 1980
81	Lysimeter and bean crop	Priestley and Taylor, 1972
77	Lysimeter and field crop	Priestley and Taylor, 1972
75	Lysimeter and grass cover	Mukammal and Neumann, 1977
66	Douglas-fir forest (High Demand)	Black and Spittlehouse, 1980
60	Douglas-fir forest	Black, 1979
60	Forest clearcut	Figure 1.4, this paper.
55	Cropped surface	Davies and Allen, 1972
50	Lysimeter and pasture crop	Priestley and Taylor, 1972
40	Bare soil surface	Estimate from Barton, 1979

α', and soil water content at different depths. Although the original approach of Priestley and Taylor was to apply their formulation to large scale environments, we apply the modified version to a small forest clearcut. A second objective was to simplify the need for extensive site-specific energy balance measurements.

METHODS

Field Methods

Data for this study were obtained during a reforestation field experiment established on the Beekman soil series (loamy-skeletal mixed mesic Typic Xerochrept) in southwest Oregon (42.72°N Lat., 123.3°W Long., 17° slope, 191° aspect, 716 meter elevation). The site had sprouting shrubs and forbs occupying 81% of the surface at the end of the measurement period (Flint and Childs, 1986) Detailed profile measurements of soil density, water content and temperature were made at ten locations and averaged for the site. Data were collected on ten sampling dates spaced every ten to twenty days from April through September, 1983.

Density of wet soil was measured using a two probe gamma attenuation device (Model 2376, Troxler Laboratories, Research Triangle Park, NC). Sampling was done in 0.025 m depth intervals starting 0.05 m from the surface. The horizontal path length for measurements was approximately 0.3 m between PVC access tubes (exact distances were measured for each measurement location). Bulk density samples were collected to convert wet density to soil water content. Soil water contents were averaged for the ten profile locations for each of the ten measurement dates.

Soil temperatures were collected every 15 minutes at five depths (0.02, 0.04, 0.08, 0.16, 0.32 m) for 1 to 3 days during the same period of time as the density measurements. At each

measurement location, a plastic probe with five thermistors (YSI #44202, Yellow Springs Instruments, Yellow Springs, OH) was installed midway between the gamma probe access tubes. Data were collected and stored in a digital data logger (Model CR-5, Campbell Scientific, Logan, UT).

Soil temperature profiles were extrapolated to estimate surface temperatures. These values were verified periodically using an infra-red radiation gun (Raynger II, Raytek, Inc., Santa Cruz, Ca). Soil heat capacities calculated from soil density and water content measurements were used with the temperature data to calculate soil heat flux using a calorimetric technique (Chapter 2).

Air temperatures were measured at 0.2 m and 2.0 m every 15 minutes over the growing season using thermistors (YSI #44202, Yellow Springs Instruments, Yellow Springs, OH) mounted in radiation shields. Dew point temperatures were measured at 0.2 and 2.0 m every 15 minutes using LiCl dewcells (Holbo, 1981).

Shortwave and net radiation were measured using a Kipp pyranometer (Kipp and Zonen, Delft, Holland) and a Thornthwaite miniature all-wave net radiometer (C. W. Thornthwaite Assoc. Camden, NJ) respectively. Data were recorded in digital format using battery powered dataloggers (Model CR-21, Campbell Scientific Inc., Logan, UT). The sensors were read every 10 seconds and integrated over 30 minutes.

Modeling Procedure

Actual evaporation was calculated using the Bowen ratio:

$$\lambda E_a = \frac{(R_n - G)}{1 + \beta} \qquad (1.2)$$

where Q^* is net radiation, G is soil heat flux, and β, the Bowen ratio, is defined as the ratio of sensible heat flux to latent heat flux. β is calculated as:

$$\beta = \frac{\rho C_p (T_1 - T_2)}{\lambda(\rho_1 - \rho_2)} \qquad (1.3)$$

where ρC_p is the volumetric heat capacity of air, λ is the latent heat of vaporization, T_1 and T_2 are air temperatures at two heights (0.2 and 2.0 m respectively), ρ_1 and ρ_2 are water vapor density at the same heights. The Bowen ratio method was used to calculate hourly values of latent heat flux.

The Priestley-Taylor equation (Eq 1.1) was modified by replacing λE_p and α with λE_a and α' respectively. This equation was rearranged to yield:

$$\alpha' = \frac{\lambda E_a}{\frac{s}{s+\gamma} \cdot (Q^* - G)} \qquad (1.4)$$

Equation 1.4 was solved on an hourly basis using Eq. 1.2 and 1.3 for λE_a, and hourly values of air temperature [for $s/(s+\gamma)$], net radiation and soil heat flux.

Although the coefficient α' could be related to any process that can limit evapotranspiration (e.g. soil hydraulic resistance, aerodynamic resistance, stomatal resistance), we chose to relate α' to soil water status by using a formulation similar to Davies and Allen (1973) and Barton (1979):

$$\alpha' = A[1-\exp(-B \frac{\theta}{\theta_s})] \qquad (1.5)$$

where A and B are regression coefficients and θ/θ_s is the current volumetric soil water content divided by the value at saturation. Davies and Allen (1972) use a soil water function in which the soil water content is divided by soil water content at field capacity (θ/θ_{fc}). The formulation of Barton (1979) simply used gravimetric water content without any scaling. In Eq 1.5 the coefficient A approaches the Priestley-Taylor coefficient (α) as the soil moisture content approaches saturation. This approach has the implicit assumption that soil water supply will be the limiting factor in actual evapotranspiration.

Measurement simplification

Measured values of net radiation (Q^*) and soil heat flux (G) were used for Bowen ratio energy budget calculations and calibration of α' for the Priestley-Taylor equation. The feasibility of using simpler or more readily available measurements of air temperature, soil temperature and incoming shortwave radiation to replace measurements of net radiation and the soil temperature profile was considered. The simplification of soil heat flux measurements by eliminating the need for soil profile measurements will be discussed in the results section.

A technique was employed to simplify the required measurements of net radiation by solving the radiation balance equation:

$$Q^* = (1-\alpha_s)K\downarrow - \epsilon_s \sigma T_s^4 + \epsilon_a \sigma T_a^4 \qquad (1.6)$$

where Q^* is net radiation, $K\downarrow$ is the incoming shortwave radiation, α_s is the surface albedo, ϵ_s is the surface emissivity, ϵ_a is the emissivity of the atmosphere and σ is the Stefan-Boltzman constant (5.67×10^{-8} W m^{-2} $°K^{-4}$). Since Q^*, $K\downarrow$, T_s, and T_a were measured, three unknowns remained (α_s, ϵ_s and ϵ_a). The atmospheric emissivity, ϵ_a, was estimated from a regression equation based on air temperature (Campbell, 1977). ϵ_s was estimated solving by Eq. 1.1. for the night time period when $K\downarrow$ is zero and terms involving α_s are eliminated. To solve for α_s, the night time value of ϵ_s was

substituted into Eq. 1.1. This equation was solved for daylight hours to estimate α_s.

RESULTS AND DISCUSSION

One example of the ten diurnal data sets analyzed is shown in Figure 1.1. A typical solution of λE_a shows the measured values using the Bowen ratio and the modeled data using the modified Priestley Taylor equation are in close agreement at midday. The apparent error in measured values of λE_a occurs at those times when the Bowen ratio (β) was near -1 (700, 1800 and 1900 hours, Figure 1.2) as would be expected by examining Eq. 1.2. Daily average values of α' were calculated using midday values of α' when $\beta > 0$. This avoided the large variation in α' calculated when the Bowen ratio method was unstable (Jury and Tanner, 1975). The magnitude of error associated with applying the midday average of α' to early and late periods of the day is small because the value of (Q^*-G) is small. The solution of Eq. 1.1 using the averaged values of α' is presented in Figure 1.1. The Bowen ratio technique could also be improved by smoothing or averaging β. We preferred, however, to use the Priestley-Taylor equation because of the smaller data requirements.

The regression coefficients A and B in Eq. 1.1 were estimated using nonlinear regression. Ten daily average values of α' were regressed against several different water content terms. In the analysis, both θ/θ_s and θ were used. In addition the values for θ and θ_s were determined for five different total soil profile depths (Table 1.3).

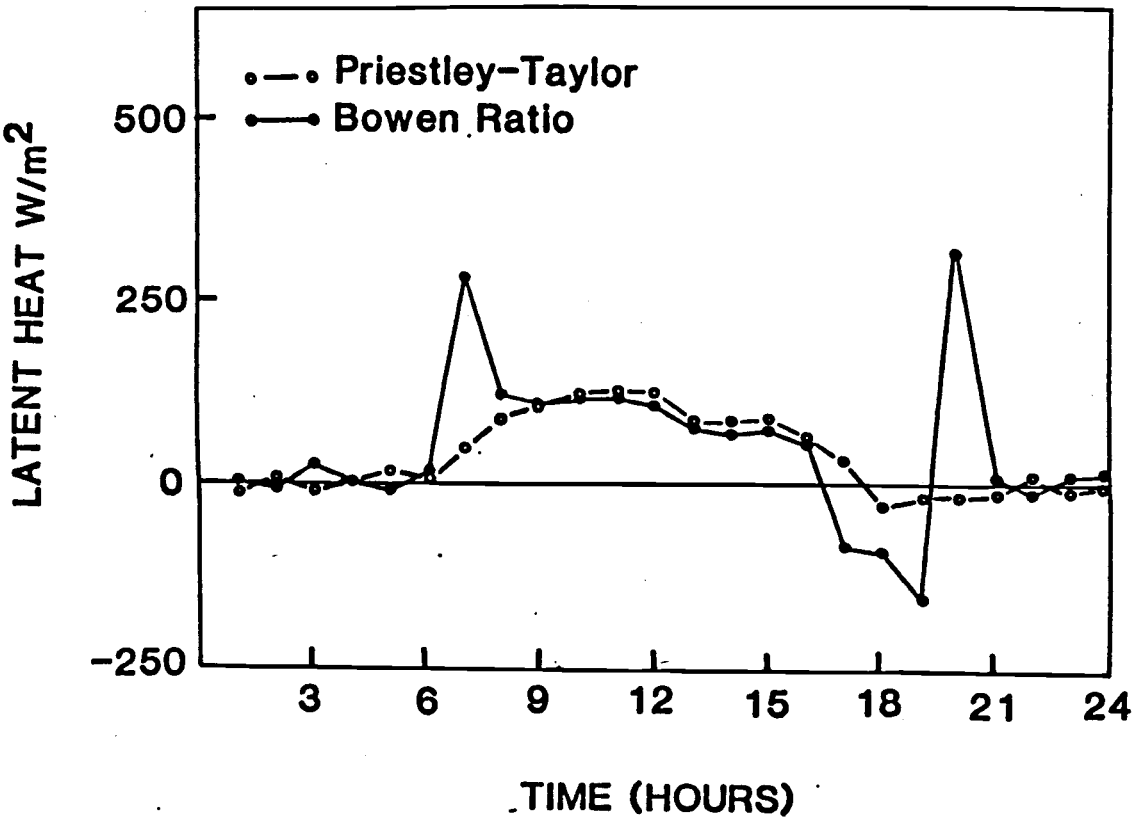

Figure 1.1 Results of latent heat flux using the Bowen ratio technique and the Priestley-Taylor technique with the daytime average value of the modified Priestley-Taylor coefficient α' for August 12, 1983, (α'=0.55).

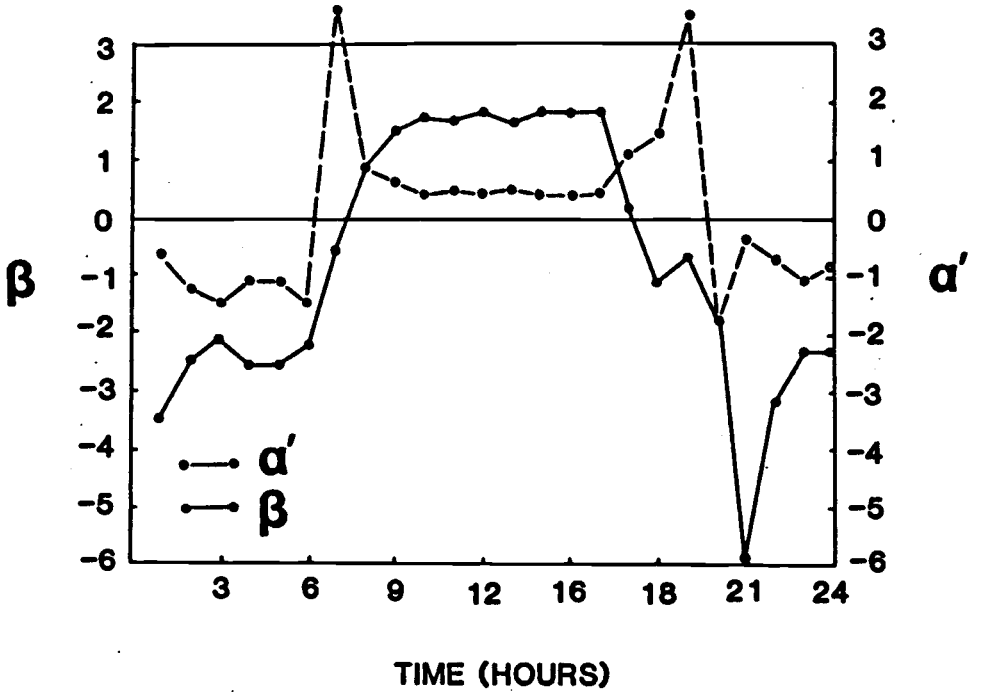

Figure 1.2 Values for the Bowen ratio (β) and for the ratio of latent heat (λE) to $(s/s+\gamma)\bullet(Q^{*}-G)$ which is equated to the Priestley-Taylor coefficient α' for nonsaturated conditions.

Use of θ or θ/θ_s made little difference in the precision of the regression results but the effect of depth of water content measurement on regression results showed interesting trends. Increased profile depth reduced the sum of squares error (SSQ) in the regression equations. The coefficient A, which should approximate the Priestley-Taylor coefficient (α) ranges from 1.08 to 1.27 as the included soil thickness goes from 0.1 to 0.5 meters. This large variation is within the range commonly measured (Table 1.1) but the sensitivity of this value to depth of measurement of soil water content discourages attaching any significant to the coefficient A.

The relationship of α' to soil water content is given in Figure 1.3 for a profile depth of 0.50 m. The regression fits the data well except at higher soil water contents. Outlier points such as these have been noted in other studies (Black, 1979) and an explanation for some outliers has been suggested. In specific, it may be inappropriate to use this modified Priestley-Taylor approach on days when the environmental demand for evaporation is low ($<12 MJ/m^2/day$) (Black, 1979). The rationale follows the observation of Denmead and Shaw (1962) that, on low demand days, even soils with low water content can supply enough water for potential evapotranspiration. In consideration of this argument we

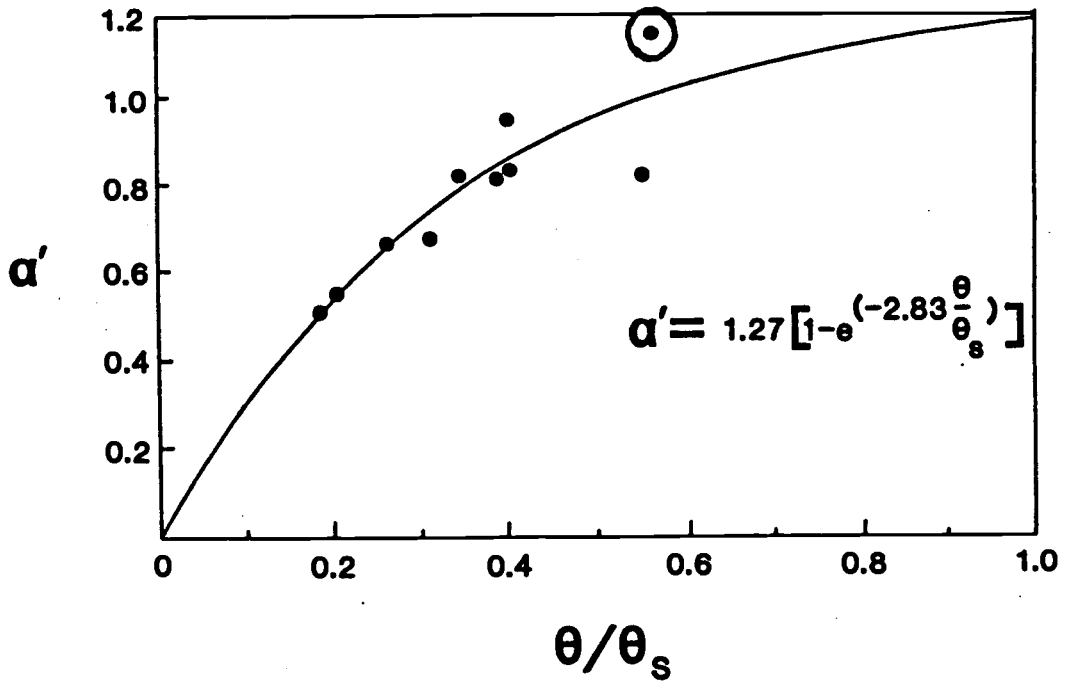

Figure 1.3 Modified Priestley-Taylor coefficient α' versus percentage of saturation (θ/θ_s, surface to 0.5 m) for the Beekman soil series at Wolf Creek, OR. The circled point indicates data collected under low environmental demand (<12MJ/m^2/day).

Table 1.3. Results of a series of regressions between α' and θ or θ/θ_s. All data points.

Depth (m)	----- θ/θ_s ----- A	B	SSQ	----- θ ----- A	B	SSQ
0-0.1	1.08	-4.06	0.1178	1.10	-8.44	0.1146
0-0.2	1.09	-4.20	0.1243	1.09	-9.48	0.1263
0-0.3	1.18	-3.41	0.1017	1.21	-7.70	0.1013
0-0.4	1.17	-3.38	0.0922	1.27	-7.19	0.0956
0-0.5	1.27	-2.83	0.0831	1.25	-7.33	0.0921

reanalyzed our data excluding values with a total radiation load of <12 MJ/m^2/day (one data point is noted in Figure 1.3). The resulting values of A (0.89 to 1.00 over the depth range, Table 1.4) were similar to the values of α found by Black (1979, Table 1.1). Excluding the one data point <12MJ/m^2/day, would yield an estimate of A $\approx$ 0.85 when the soil is near field capacity ($\theta/\theta_s \approx 0.6$).

A simplified solution to the formulation of α' would be to set an upper limit of $\alpha' = 0.85$ where $\lambda E_p = \lambda E_a$. α' could be reduced when soil water content falls below some critical value of θ/θ_s where soil water supply limits evapotranspiration. By estimating total available water content as the difference between field capacity ($\theta/\theta_s \approx 0.60$) and driest seasonal water content ($\theta/\theta_s \approx 0.18$) it can be seen that when more than 60 percent of this total available water is used, ($\theta/\theta_s \approx 0.35$, Figure 1.3), soil water becomes limiting. This value is in general agreement with the data in Table 1.2. Although further analysis is needed to properly evaluate α' when the soil is at field capacity for our soil, the relationship between α' and θ/θ_s below field capacity would remain the same.

The Priestley-Taylor equation can be used with measured data to calculate evapotranspiration under dry soil conditions. Still, the method requires measurements or estimates for net radiation and soil heat flux. Because these data are not commonly collected for reforestation sites, the potential for replacing the measurements with estimate was considered. Soil heat flux measurements are

Table 1.4. Results of a series of regressions between α' and θ_2 or θ/θ_s for all data points with daily total net radiation >12MJ/m^2.

Depth (m)	----- θ/θ_s ----- A	B	SSQ	----- θ ----- A	B	SSQ
0-0.1	0.89	-6.30	0.0559	0.89	-13.58	0.0553
0-0.2	0.88	-6.63	0.0642	0.89	-14.64	0.0654
0-0.3	0.93	-5.42	0.0490	0.94	-12.39	0.0481
0-0.4	0.96	-4.82	0.0378	0.96	-11.81	0.0443
0-0.5	1.00	-4.18	0.0371	0.97	-11.73	0.0408

probably not required because heat flux values are small in comparison to net radiation. A common simplification is to estimate soil heat flux as a constant percentage of net radiation. Measurements from this study indicate that values between 15 and 25 percent would be appropriate. This range is higher than the 10 percent values commonly assumed for daytime conditions (e.g. Campbell, 1977) and is probably larger because of the high rock fragment percentage of these soils (See Chapter 2).

Simplification of net radiation measurements can be accomplished using the radiation balance equation (Eq. 1.6). An example diurnal radiation balance for the site (Figure 1.4) shows the magnitude of the major terms in the equation. It appears that incoming solar radiation is most closely correlated with net radiation because of the compensating effects of incoming and outgoing longwave radiation. In Chapter 3, a procedure is presented for predicting solar radiation from slope, aspect, elevation and surrounding topography. Tests of the procedure using data from six sites showed it to be excellent for estimating radiation. The albedo and emissivity terms of Eq. 1.6 were derived using the procedure outlined earlier. Results of the technique employed for 10 cloud free days over the growing season showed no apparent seasonal variation in α_s or in ϵ_s. The value found for ϵ_s, 0.98, is reasonable for a dry soil surface and the value of α_s, 0.26, is in agreement with a directly measured value ($\alpha_s = 0.30$) for the same soil series (Holbo et al, 1986).

The radiation balance (Eq. 1.6) can be used to estimate net radiation in the following manner:

1) Calculate solar radiation using a calibrated model (Chapter 3).
2) Estimate α_s and e_s using a 24 hour data set consisting of air temperature, soil temperature and net radiation.
3) Use measurements or estimates or air and soil temperature for each day net radiation estimates are required.

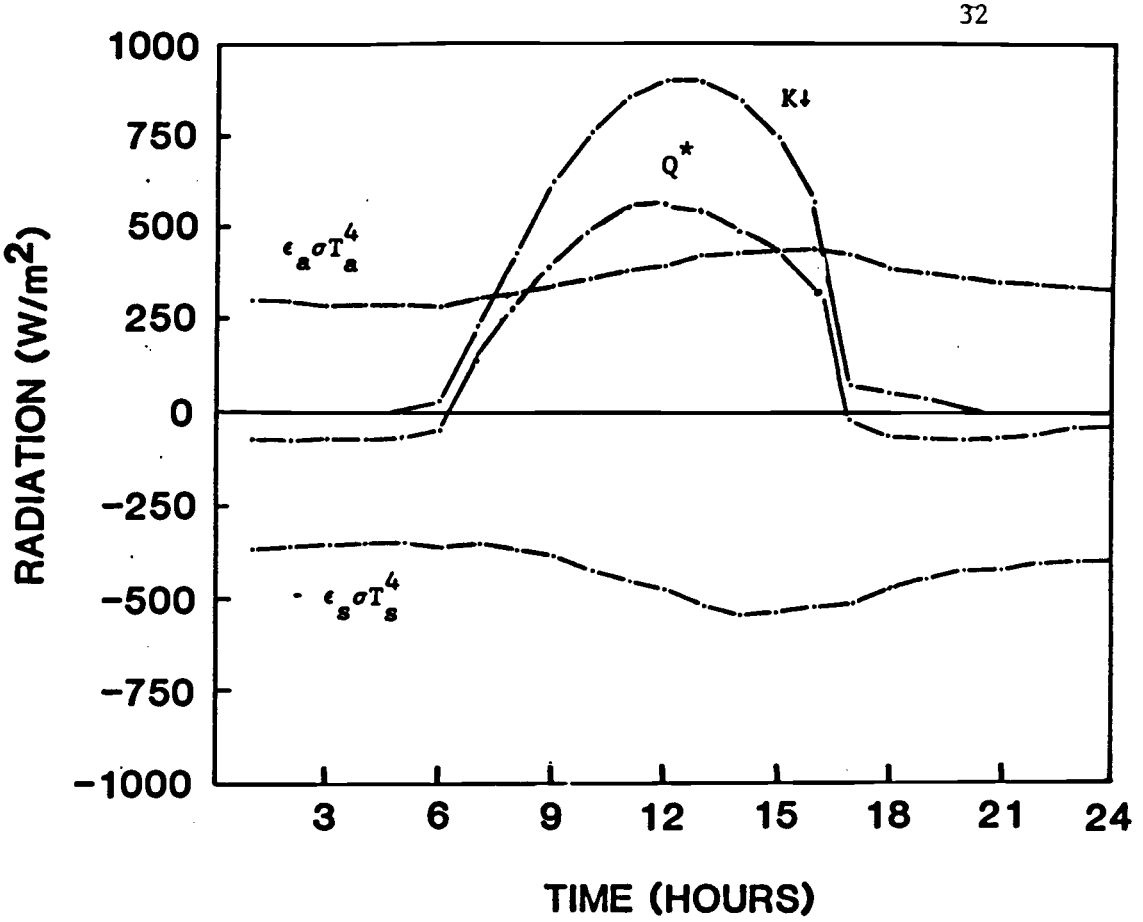

Figure 1.4 The radiation balance for the Wolf Creek site, August 12, 1983. $\alpha K\downarrow$ is incoming short wave radiation, $\epsilon_a \sigma T_a$ is incoming longwave radiation, $\epsilon_s \sigma T_s$ is outgoing longwave radiation and Q^* is net radiation.

CONCLUSIONS

The Priestley-Taylor equation can be adequately modified to calculate actual evaporation by incorporation of α' as a variable dependent on soil water content. The formulation of the relationship between and soil water content can be described by an exponential equation. The coefficients for the exponential equation, A and B, are dependent on the depth of measurement for soil water content and the environmental demand for water. The best results for our formulation of the soil water function were when soil water content was averaged from the surface to 0.50 m and by excluding any data point with total radiation less than 12 MJ/m^2.

Four measurements suggested (Q^*, G, air temperature and soil water content) are required for the modified Priestley-Taylor method. The model reduces the need to measure the air temperature and vapor density profiles for the Bowen ratio method or the more extensive measurements required for the Penman and Penman-Monteith equation. Measurement of Q^* can be replaced by measurement of air temperature, soil surface temperature and measured or modeled values of solar radiation. With this approach, the Priestley-Taylor model can be applied on a seasonal basis to predict water loss with good results for a variety of site locations. If models of soil heat flux and solar radiation are used, the only measurements or estimates required to characterize a site for reforestation microclimate are air and soil temperatures.

REFERENCES

Barton, I. J., 1979. A parameterization of the evaporation from nonsaturated surfaces. Journal of Applied Meteorology. 18:43-47.

Black T. A., 1979. Evapotranspiration from Douglas-fir stands exposed to soil water deficits. Water Resources Research. 15(1):164-170.

Black, T. A. and D. L. Spittlehouse. 1980. Modeling the water balance for watershed management. p. 117-129. In: D. M. Baumgartner, (Ed.), Interior West Watershed Management. Washington State University. Pullman, Washington.

Campbell, G. S., 1977 An Introduction to Environmental Biophysics Springer-Verlag, New York, 159 pp.

Davies J. A. and C. D. Allen, 1973. Equilibrium, potential and actual evaporation from cropped surfaces in southern Ontario. Journal of Applied Meteorology. 12:649-657.

De Bruin H. A. R. 1983. A model for the Priestley-Taylor parameter α. Journal of Climate and Applied Meteorology. 22:572-578.

De Bruin, H. A. R., and A. A. M. Holtslag, 1982. A simple parameterization of the surface fluxes of sensible and latent heat during daytime compared with the Penman-Monteith concept. Journal of Applied Meteorology. 21:1610-1621.

Denmead, O. T., and R. J. Shaw. 1962. Availability of soil water to plants as affected by soil moisture content and meteorological conditions. Agron. J. 54:385-390.

Giles, D. G., T. A. Black, and D. L. Spittlehouse. 1985. Determination of growing season soil water deficits on a forested slope using water balance analysis. Can. J. For. Res. 15:107-114.

Holbo, H. R., 1981. A dew-point hygrometer for field use. Agric. Meteorol. 24:117-130.

Holbo, H. R., S. W. Childs, and E. L. Miller. 1986 Summertime radiation balances of clearcuts and shelterwood slopes in southwest Oregon. Forest Science. Submitted.

Jury, W. A. and C. B. Tanner. 1975. Advection modification of the Priestley and Taylor evapotranspiration formula. Agronomy Journal 67:840-842.

McNaughton, K. G., and T. A. Black, 1973. A study of evapotranspiration from a Douglas-fir forest using the energy balance approach. Water Resources Research. 9:1579-1590.

Monteith, J. L. 1964. Evaporation and environment. In The Stat and Movement of Water in Living Organisms. 19th Symp. Soc. exp. Biol., 205.

Mukammal, E. I. and H. H. Neumann, 1977. Application of the Priestley-Taylor evaporation model to assess the influence of soil moisture on the evaporation from a large weighing lysimeter and class A pan. Boundary Layer Meteorology. 12:243-256.

Penman, J. L.. 1948. Natural evaporation from open water, bare soil and grass. Proc. Roy. Soc. London. A193:120-145.

Priestley C. H. B. and R. J. Taylor, 1972. On the assessment of surface heat flux and evaporation using large-scale parameters. Monthly Weather Review. 100(2):81-92.

Shuttleworth, W. J. and I. R. Calder. 1979. Has the Priestley-Taylor equation any relevance to forest evaporation? Journal of Applied Meteorology. 18:639-646.

Stewart, R. B., 1983. A discussion of the relationships between the principal forms of the combination equation for estimating crop evaporation. Agric. Meteorol., 30:111-127.

Stewart, R. B. and W. R. Rouse, 1977. Substantiation of the Priestley and Taylor parameter α=1.26 for potential evaporation in high latitudes. Journal of Applied Meteorolgy. 16:649-650.

Tanner C. B. and W. A. Jury. 1976. Estimating evaporation and transpiration from a row crop during incomplete cover. Agronomy Journal. 68:239-243.

2. Estimating Thermal Properties of a Forest Soil

Alan L. Flint and Stuart W. Childs

Department of Soil Science

Oregon State University

Estimating Thermal Properties of a Forest Soil[1]

Alan L. Flint and Stuart W. Childs[2]

ABSTRACT

Intensive measurement of soil temperatures, soil densities, and water contents are required to precisely define the thermal environments of heterogeneous forest soils. Fifty detailed profiles of temperature, density, and water content were used with the conduction heat flow equation to estimate soil thermal properties for a clear cut harvest area in a mixed conifer forest in southwest Oregon. This data set was used to determine the

---

[1]Oregon Agric. Exp. Stn. Technical paper no.____. Contribution of the Dept. of Soil Science, Oregon State Univ., Corvallis, OR. This work was supported as part of the Forestry Intensified Research Program (PNW-80-85), a cooperative project of Oregon State University, the USDA Forest Service, and the USDI Bureau of Land Management.

[2]Graduate Research Assistant and Assistant Professor, respectively, Dept. of Soil Science, Oregon State University, Corvallis, OR 97331.

accuracy with which soil temperatures could be modeled and the number of measurements required to characterize a given field site. The soil was modeled as a profile of between one and twenty one layers of known (measured) volumetric heat capacity and measured initial and boundary conditions. Soil thermal conductivity for each layer was determined for each data set using an iterative numerical procedure. The accuracy of the various models was assessed by comparing root mean square error between measured and modeled profiles. For the skeletal soil studied, a model and field measurements of four soil layers proved to be the best combination of accuracy and simplicity. The assumption of a homogeneous (one layer) profile was acceptable in a number of cases.

The value of added detail in field measurements for a specific soil was determined by estimating soil temperature parameters of importance: minimum and maximum temperature, duration of high temperature and low temperature events, and positive and negative heat flux. Models of four or more soil layers were within 0.3°C of measured temperatures. Models with two or more soil layers were within 0.006 $MJ/m^2/day$ in matching positive heat flux.

INTRODUCTION

Soil temperature plays a significant role in seedling establishment on forest soils. High soil temperatures in late summer may cause seedling heat stress or mortality (Arnott, 1975; Childs and Flint, 1986; Hallin, 1968) while low soil temperatures in early spring slow root and shoot growth (Lopushinsky and Kaufmann, 1984) as well as seedling bud burst (Sorensen and Campbell, 1978). This delay in initiation of growth can be critical in situations where the duration of adequate soil water supply is short (Flint and Childs, 1984a). Dobbs and McMinn (1977) found that elevated soil temperatures, created by removal of surface organic layers, benefited planted seedling establishment during the growing season in British Columbia.

There are other effects of soil temperature on the environment for seedling growth. Large diurnal fluctuations in soil temperature can occur in dry, low heat capacity soils. These fluctuations cause depth gradients which allow deep soil heating and movement of water to the surface at night where it can evaporate during the day (Mehuys et al., 1975; de Vries, 1963). Rates of biological activity and chemical reactions change with temperature. Beneficial effects of warm soil temperatures include increased phosphorous availability (van den Driessche, 1984) and increased nitrogen mineralization rate (Milthorpe and Moorby, 1974). Delay of mycorrhizal establishment (Parke et. al., 1984) can be a detrimental effect of soil temperatures above 24°C or

below 18.5°C. These considerations make proper management of soil temperature important for seedling establishment and growth, particularly on environmentally harsh sites.

Temperature distribution in a soil is established by heat flow, which is determined by the combined effect of soil thermal properties and the soil surface energy balance. Energy exchange at the soil surface is the primary source of heating and cooling for the soil profile. Environmental conditions account for both the magnitude and the timing of soil heat flux.

The thermal properties of major importance to heat flow in soils are heat capacity and thermal conductivity. Whole-soil heat capacity, the heat storage per unit temperature change, is calculated as sum of the heat capacities of the individual soil constituents. Water is the soil constituent with the highest specific heat and is therefore an important component of whole soil heat capacity. Thermal conductivity, the rate of heat transfer per unit temperature gradient, is determined by both component thermal conductivities and their arrangement in space. Thermal conductivity can be calculated from equations relating bulk soil properties of water content, bulk density, and porosity as well as the thermal conductivity of individual soil particles and their shape and orientation in the soil (de Vries, 1963).

Estimates of thermal conductivity in forest soils are particularly difficult because of soil heterogeneity due to rock fragments and layering of organic matter and surface litter. Soil density and water content vary considerably with depth, largely due

to the presence or absence of rock fragments. Rock fragments influence heat transfer in wet soils by reducing total porosity and also by restricting drainage to increase early season soil water content (Flint and Childs, 1984b). In wet soils the presence of rock fragments can either increase or decrease heat capacity but thermal conductivity is usually increased. In dry soils, where reduction of total porosity has little effect on water content, both heat capacity and thermal conductivity are increased.

Soil thermal diffusivity, the ratio of thermal conductivity to heat capacity, is used in many numerical methods to predict soil temperatures (Hanks et al, 1971; Horton et al, 1983). Often, however, the thermal diffusivity is not known and must be estimated. Although a number of measurement techniques have been used, many researchers currently use techniques involving inverse solution of the soil heat flow equation for homogeneous soils using numerical methods (Firdaouss et al., 1983; Horton et al., 1983). Few researchers have applied such methods to heterogeneous soils.

OBJECTIVE

The goal of this study was the development of methods and measurements required for accurate estimates of soil thermal properties for use in calculations of the surface energy balance, soil heat flux, and soil temperature profiles. This goal necessitated two research objectives. First, a formulation of the

inverse solution to the conduction heat transfer equation must be combined with measured soil temperatures and properties to calculate thermal conductivity for heterogeneous soils. Second, the intensity of measurements and modeling required for various fundamental and applied calculations must be assessed.

METHODS

Field Methods

Data for this study were obtained during a reforestation field experiment established on the Beekman soil series (loamy-skeletal mixed mesic Typic Xerochrept) in southwest Oregon (42.72°N Lat., 123.3°W Long., 17° slope, 191° aspect, 716 meter elevation). The site had sprouting shrubs and forbs occupying 81% of the surface at the end of the measurement period (Flint and Childs, 1986) Detailed profile measurements of soil density, water content and temperature were made at ten locations and averaged for the site. Data were collected on ten sampling dates spaced every ten to twenty days from April through September, 1983.

Density of wet soil was measured using a two probe gamma attenuation device (Model 2376, Troxler Laboratories, Research Triangle Park, NC). Sampling was done in 0.025 m depth intervals starting 0.05 m from the surface. The horizontal path length for measurements was approximately 0.3 m between PVC access tubes (exact distances were measured for each measurement location). Bulk density samples were collected to convert wet density to soil water content. Soil water contents were averaged for the ten profile locations for each of the ten measurement dates.

Soil temperatures were collected every 15 minutes at five depths (0.02, 0.04, 0.08, 0.16, 0.32 m) for 1 to 3 days during the same period of time as the density measurements. At each

measurement location, a plastic probe with five thermistors (YSI #44202, Yellow Springs Instruments, Yellow Springs, OH) was installed midway between the gamma probe access tubes. Data were collected and stored in a digital data logger (Model CR-5, Campbell Scientific, Logan, UT).

A typical profile of soil density is presented in Figure 2.1a for two moisture contents: field capacity and the driest profile of the season. The difference between the wet and dry curves indicates net seasonal soil water loss. The marked variation in density with depth is due primarily to the presence of rock fragments and the retention of soil water above rock layers.

Heat capacity was calculated as the sum of the heat capacities of the soil minerals and water. Equation 2.1 shows the calculation of volumetric heat capacity (C_s) from soil bulk density (ρ_b), volumetric water content (θ_v) and particle density (ρ_p), all in units of Mg/m^3.

$$C_s = [C_m(\rho_b/\rho_p) + C_w(\theta_v)]\cdot\rho_b \qquad (2.1)$$

Soil mineral heat capacities (C_m) were assumed to be 1.47 MJ/Mg°K based on calorimetric determinations for similar soils (Childs et al., 1985), and soil water heat capacity (C_w) was assumed to be constant, 4.18 MJ/Mg°K. The increased heat capacity for soils with large percentages of rock fragments are accounted for in the increased bulk densities of the soils since there is little

difference between heat capacities of rock fragments and soil minerals measured on a weight basis (Childs et al., 1985).

Using measurements of soil density and water content, such as Figure 2.1a, the heat capacity for the soil was calculated in 0.02 m depth increments (Figure 2.1b). The high heat capacity of water (compared to mineral soil) has a large effect on soil heat capacity on a seasonal basis. Calculation of soil heat capacity did not account for the small organic matter contents of our soils because it was found that their contribution to total heat capacity was minor (<5%) compared to the high heat capacity and large field variability of water content.

Calculation of thermal conductivity

An explicit-implicit finite difference numerical method similar to that of Riha et al. (1981) was used to solve the transient state, conduction heat flow equation. Required inputs are: 1) an initial soil temperature profile, 2) a heat capacity profile, 3) variation of soil temperature with time for the upper profile boundary condition, and 4) soil temperature of the deepest soil layer modeled. In this study, measured 0.02 m temperature was used for the upper boundary temperature input. The deepest layer (0.44 m) was assumed to be at a constant temperature equal to the mean temperature measured at 0.32 m over the period of data collected.

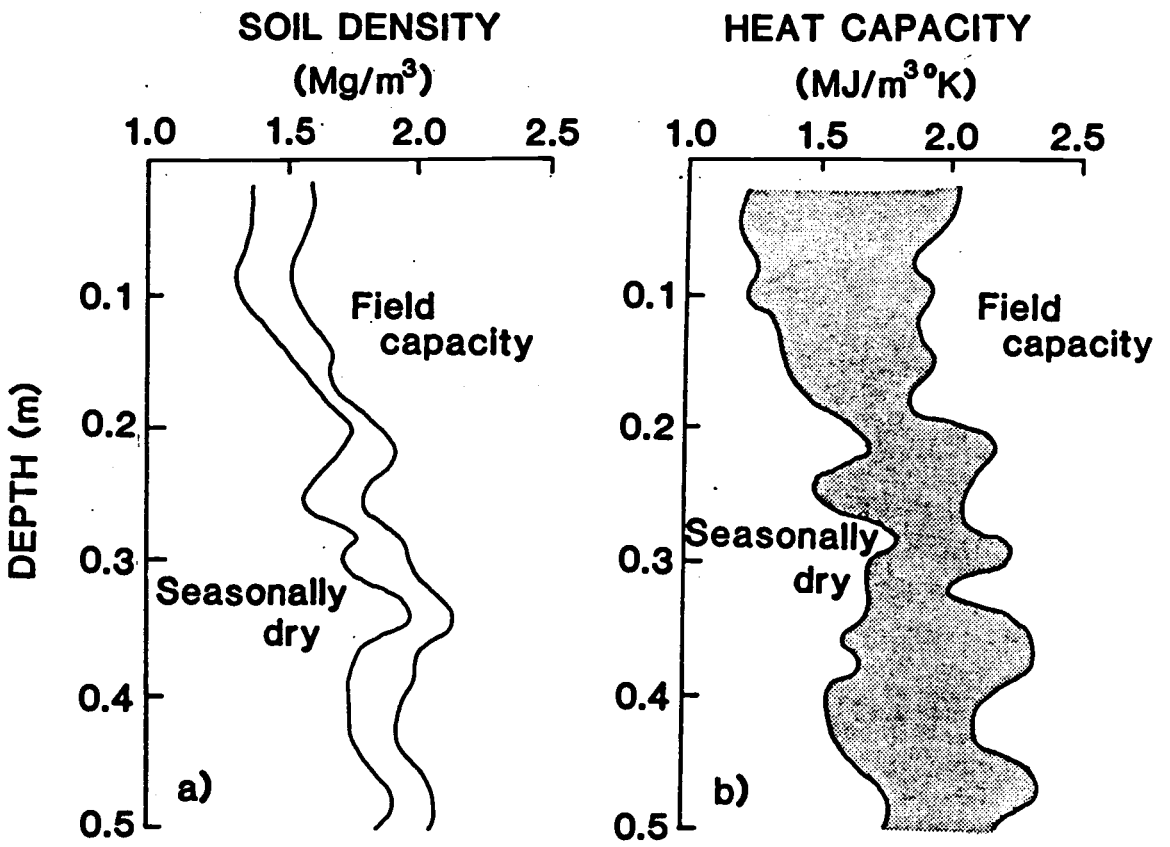

Figure 2.1 Range in wet soil density (a) and heat capacity (b) at field capacity (early spring) and at the driest time of the year (late summer). The difference in wet density is net soil water loss for the season.

The soil profile was divided into twenty one 0.02 m increments from 0.02 to 0.44 m depth for the numerical method. This depth resolution is the same as that of the field measurements of soil properties. Calculations were made for all layers in the most detailed model of the soil profile. In addition, calculations were made assuming that the soil profile was made up of a smaller number of layers. Calculations for one, two, four, seven, ten, and twenty one layers were made and analyzed.

A trial and error procedure was used to select the proper soil thermal conductivity profile for each dataset. Measured profiles of heat capacity and an estimate of thermal conductivity were used to calculate temperatures at the same depths and times as those of the field measurements. The goodness of fit of the calculated temperatures to the measured values was assessed using a residual error term (RE):

$$RE = \sum_{i=1}^{N} \sum_{j=1}^{M} (T_m - T_c)^2 \qquad (2.2)$$

where T_m is the measured temperature, T_c is the calculated temperature, N is the number of 15 minute intervals, and M is the number of thermistor sensors, excluding the 0.02 m sensor which is used as the upper boundary condition ($\therefore$ M=4).

In the one layer model the soil was considered to be homogeneous and heat capacity and thermal conductivity are held constant with depth. We simulated this by averaging our detailed

heat capacity information from the entire profile. This single value of heat capacity was used in the numerical method to select the thermal conductivity which best matched the temperature data set in the following manner:

1) Start with a low value of thermal conductivity (0.1 $W/m^2°K$) for the one layer soil model and calculate residual error (Eq. 2.2).

2) Increase the value of thermal conductivity in the soil by 0.1 $W/m^2°K$ and recalculate soil temperatures and residual error.

3) Continue to increase thermal conductivity in step 2 until the residual error term is minimized.

The solution represents the best estimate of thermal conductivity for the "one layer" or "homogeneous" soil.

A two layer soil profile was modeled by dividing the conductivity and heat capacity values into two layers above and below the 0.09 m depth. This depth division placed two thermistors in the upper soil layer (at 0.04 and 0.08 m) and two in the lower soil layer (0.16 and 0.32 m). Heat capacity values were calculated by averaging measured values from the 0.01 m to 0.09 m for the surface layer and 0.09 m to 0.44 m for the subsurface layer. The following procedure was then used to calculate the thermal conductivities for the two layer soil:

1) Use the "one layer" thermal conductivity as the first estimate of thermal conductivity for the subsurface layer.

2) Vary the thermal conductivity of the surface layer in increments of 0.1 $W/m^2°K$ until the error term is minimized.

3) Set the thermal conductivity of the surface layer at this optimum value.

4) Vary the thermal conductivity of the subsurface layer in increments of 0.1 $W/m^2°K$ until the residual error term is minimized.

5) Repeats steps 2, 3 and 4 for several iterations ($\approx$ 4) until the error term in minimized by the best combination of upper and lower layer thermal conductivities.

The result is an estimate of the two layer profile of thermal conductivity to a resolution of 0.1 $W/m^2°K$.

An analogous solution procedure was continued with more complex physical models of the soil (four, seven, ten and twenty-one layers). The four layer model was designed to incorporate each temperature sensor (0.04, 0.08, 0.16 and 0.32 m depths) at the center of a soil layer. The seven, ten and twenty-one layer models were used to determine the resolution of soil properties needed to predict temperature and heat flow. The

number of iterations required for the multi-layered models were not large (≈4 to 7) because each model used initial thermal conductivity estimates taken from the results of the previous models of lesser complexity.

Calculation of soil temperature

In order to analyze the usefulness of the models in predicting soil temperature and heat flux, predicted values of soil temperatures were calculated from the solution of each model for each dataset. Predicted and actual maximum and minimum temperatures for each measurement depth (0.04, 0.08, 0.16, 0.32 m), were compared. Also, ability to predict the times of occurrence of that maximum or minimum temperature was assessed. A second part of the analysis was to determine the effectiveness of the models in predicting the duration of soil temperatures in certain ranges. This was done by comparing the duration the measured soil temperatures remained above or below a certain critical temperature with model results. The range tested was the optimum range for mycorrhizal development (18.5°C to 24°C; Parke et al., 1984).

Calculation of soil heat flux

Heat flux density was calculated using a calorimetric approach:

$$HSR = \sum_{i=1}^{4} C_{si} \cdot \Delta Z_i \cdot \Delta T/\Delta t \qquad (2.3)$$

where HSR is the hourly heat storage rate ($MJ/m^2/sec$), C_{si} is the heat capacity of the i^{th} soil layer (including water), ΔZ_i is the thickness of the i^{th} layer, and ΔT is the change in temperature during Δt, the time increment. Depth layers centered on the thermistor depths were used in evaluation of all models: 0.01-0.03, 0.03-0.06, 0.06-0.12, 0.12-0.24, 0.24-0.44 m.

RESULTS AND DISCUSSION

The accuracy of model results was not influenced by the spatial distribution of the ten soil profile locations or by the seasonal distribution of the measurements. The fifty data sets were, therefore, analyzed as a group. The actual values of thermal conductivity do vary both with depth and time. The significance of these trends to model selection and results will be discussed later.

Thermal conductivity profiles increased in complexity as the number of modeled soil layers increased. Figure 2.2a is a typical profile for thermal conductivity as calculated by three models of different complexity. Since the greatest change in temperature is near the surface and three of the four sensors are within 0.16 m of the surface this depth range most strongly influenced the optimum thermal conductivity value selected by the one layer model. When the two layer soil model is used, the thermal conductivity of the deeper soil is better represented.

Results of the ten and twenty one layer models showed lower than expected thermal conductivities for the deepest layers. This result may be an artifact of the solution technique employed. These low values of thermal conductivity were selected by the modeling procedure for the layers below the deepest temperature sensor (0.32 m) because changes in thermal conductivity at those depths had an effect on temperatures smaller than the resolution of

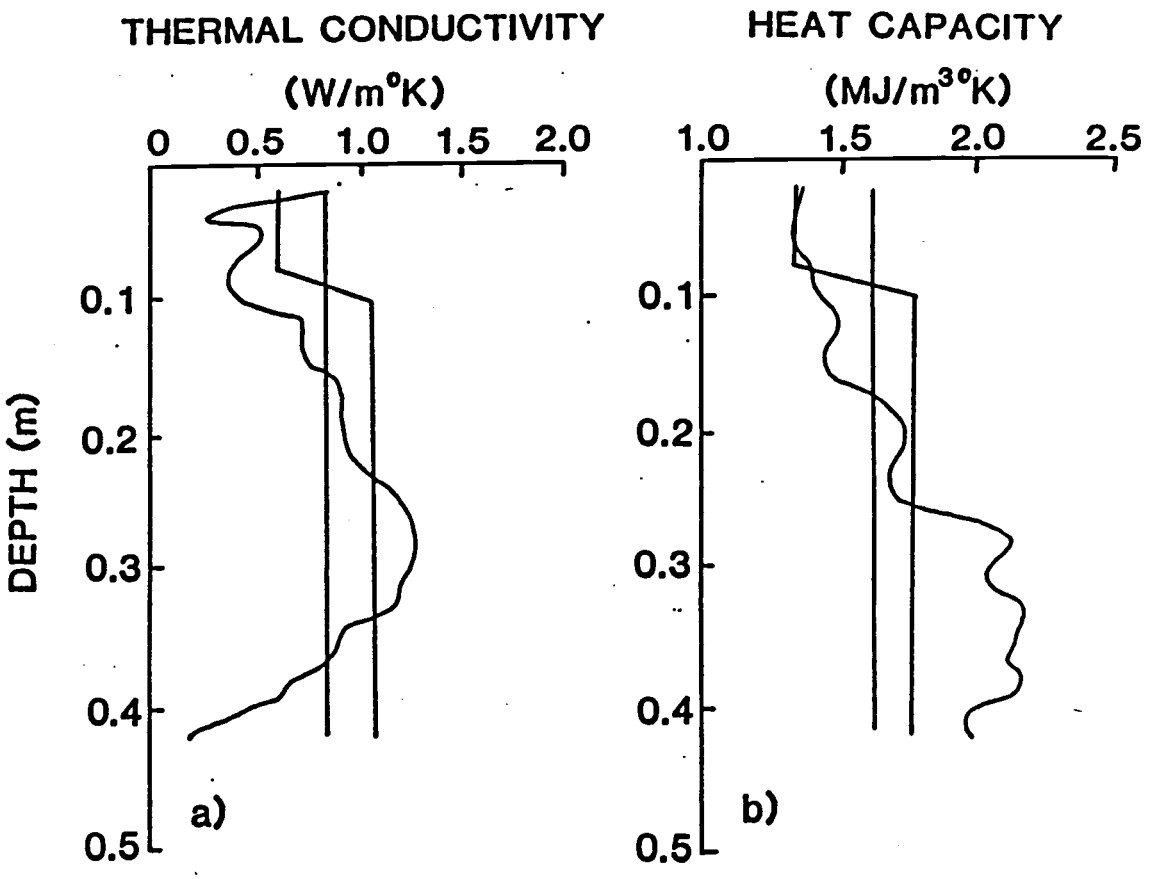

Figure 2.2 Depth profiles of measured heat capacity (b) and model values of thermal conductivity (a) calculated using one, two and twenty-one layer models.

the measurements. Thermal conductivities calculated below about 0.35 m are therefore probably not reliable.

The heat capacity profiles from the same location as Figure 2.2a are shown in Figure 2.2b. The magnitudes are representative of dry skeletal soil. The averaged profiles used in the one and two layer models do not closely follow the detailed profile. In particular the fit at 0.25 to 0.40 m is poor.

Two tests were used to assess the performance of the various models. First, a paired T-test was used to quantify differences in residual error (Eq 2.2) between models. Increasing the complexity of the soil model from one layer to twenty-one layers decreased residual error. The reduction in error between the one and two layer models was, however, not statistically significant (Table 2.1) due to the large standard error. Since each series of measurements have different time durations (1 to 3 days), mean values for residual error were not compared, only differences. A representative value of residual error for the one layer model over one day would be ≈ 75.

The second test performed was based on the absolute value of the mean difference between measured and calculated temperature:

$$ME = SQR\left(\sum_{i=1}^{50} (RE / N / 4)\right) \qquad (2.4)$$

where ME is the mean error, RE is the residual error from Eq. 2.2, N is the number of 15 minute intervals (N averaged 130 and ranged

Table 2.1. Results of paired T-test between models (N=50). These values show the mean reduction in the residual error term (RE, Eq. 2.2) when comparing one model to the next, more complex model.

	Number of Layers				
	one vs two	two vs four	four vs seven	seven vs ten	ten vs twenty-one
Mean	21.0	25.0†	3.0†	3.9†	3.9†
Standard error	11.3	5.1	0.7	0.6	1.2

†Statistically different at the 0.05 level.

between 60 and 226) and 4 is the number of sensors originally summed into equation 2.2. This calculation technique does not account for any bias among the temperature sensors.

There is a reduction in the mean error term (ME) with increasing complexity of the model but discerning statistically differences between the smaller values, which are approaching the sensitivity of the measurements (0.1°C), is more difficult. There is still an improvement ($\approx$ 0.1°C per depth per time increment) in modeling the thermal conductivity of the soil by including at least four soil layers (Tables 2.1 and 2.2) compared to the one layer model. The mean error is, however, low for all models (<0.4°C).

The lack of seasonal trends in model results does not indicate a lack of seasonal variability in temperature or thermal properties. During midsummer, the maximum measured temperature exceeded 40°C at 0.02 m and 22°C at 0.32 m while both early spring and fall minimum temperatures were less than 8°C at 0.02 m and less than 12°C at 0.32 m. This range constituted a realistic and appropriate test for the models. Considering this range and a measurement resolution of 0.1°C, the overall mean errors for the one and two layer models (0.4°C) and four or more layers (0.3°C) are small. This error in predicted temperature is acceptable for many applications.

The data of Tables 2.1 and 2.2 indicate that a model including four layers and, therefore, four measurements of soil properties provides a good balance between model complexity and detail of soil characterization. Since a common use of soil temperature models is

Table 2.2. Mean error in temperature per 15 minute time interval per depth in °C. Results of T-test are for the difference between any two means (Mean error = SQR(Σ(RE/N/4), Eq 2.4).

	Number of layers					
	one	two	four	seven	ten	twenty-one
Mean‡	0.43	0.38	0.33	0.33	0.31	0.29
Standard deviation	0.25	0.19	0.17	0.17	0.17	0.15

‡Model results are not statistically different from each other at the 0.05 level.

the prediction of soil temperatures, the models were compared based on the accuracy of prediction of: 1) maximum temperature, 2) minimum temperature, 3) time of maximum temperature, 4) time of minimum temperature and 5) duration of soil temperature outside an arbitrary range.

In considering the worst case in predicting maximum temperature, the one and two layer models were still within 2°C whereas with four or more layers the errors were within 1.5°C. In predicting minimum temperature, the one and two layer models were within 1.5°C whereas models using four or more soil layers were within 1°C of measured data. On the average the one and two layered models were within 0.3°C whereas models with four or more layers predicted within 0.2°C for either maximum or minimum temperature. All models reached the daily maximum and minimum temperatures within two to three time increments (30 to 45 minutes) of the measured data.

Evaluation of the models in predicting duration above or below specified temperatures provided some useful information to help distinguish among models (Table 2.3). The one and two layer models were the least effective in calculating the proper duration at 0.04 and 0.08 m. The twenty-one layer model provided the best estimate at 0.16 m and all the models equally predicted duration at 0.32 m. Once four layers are used in the model there is little additional improvement by using more detailed models.

A final test of the utility of various models was made by comparing predictions and measurements of soil heat flux. Positive

Table 2.3. Percentage of time the model was more than one hour in error in predicting the duration of soil temperature outside of the optimum range for mycorrhizal development (18.5° to 24.0°C). The analysis is based on 44, 24 hour data sets.

Depth (m)	Models layers					
	one	two	four	seven	ten	twenty-one
	%					
0.04	7	10	2	2	2	2
0.08	27	27	20	18	16	16
0.16	29	27	27	27	27	21
0.32	7	9	9	9	9	9

and negative heat flux were examined separately because of the major differences in their values and durations. It is of note that, with soil surface temperatures over 40°C in early spring, hourly positive heat flux values exceeded 400 W/m^2 (Figure 2.3), which was more than half of the net radiation at that time. The high thermal diffusivities calculated for the soil during this same time period also indicate strong and rapid heating of the soil profile (Table 2.4). However, the duration of positive heat flux was short and large negative values of night time heat flux ($\approx$ -175 W/m^2), kept daily net heat flux near zero (Figure 2.3). Both daily and hourly heat flux values were adequately predicted by all models for many purposes (the one layer model results are shown in Figure 2.3).

The evaluation of positive heat flux provided the most information to distinguish among models. The one layer model had an average error in prediction of total positive heat flux of less than 0.010 $MJ/m^2/day$. All other models were significantly lower (<0.006 $MJ/m^2/day$) but not different from each other.

The moisture and density conditions used in the four layer model and the solution for thermal conductivity provide more information in support of having at least four soil layers in the model. There are distinctly different soil densities and early season water contents in the four soil layers which lead to the calculated differences in heat capacity and thermal conductivity profiles (Table 2.4). The higher water content at all depths early in the spring makes a significant contribution to thermal

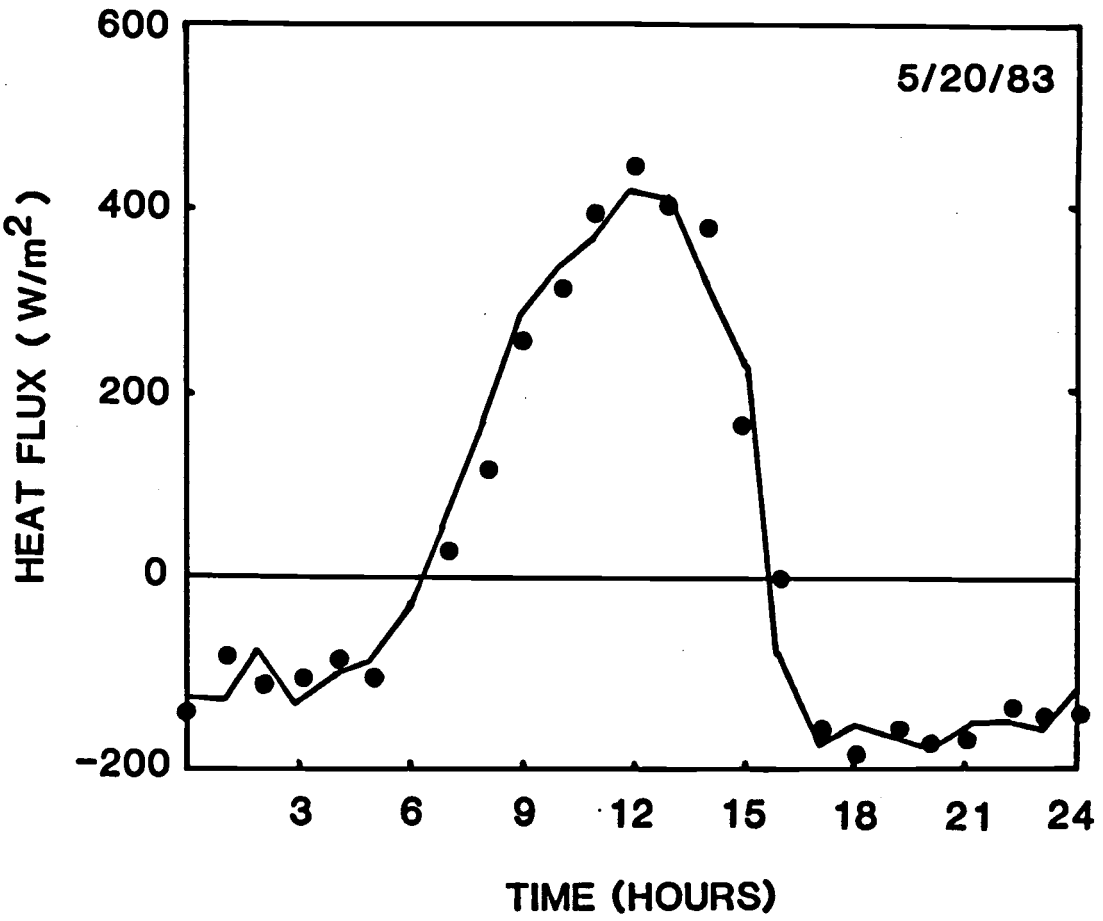

Figure 2.3 Measured soil heat flux (•) and the results of the one layer model of soil heat flux (—). Total positive heat flux is 8.80 MJ/m^2, total negative heat flux is 6.64 MJ/m^2 and total net heat flux is 1.36 MJ/m^2.

Table 2.4. Soil bulk density, seasonal range of soil water content and soil thermal properties of conductivity, heat capacity, and diffusivity. Values are from the four layer model and are means plus or minus one standard deviation (N=5).

†Model Layer	Thermal Conductivity	Heat Capacity	Thermal Diffusivity	Bulk Density	Water Content
	$Wm^{-2}{}^{\circ}K^{-1}$	$MJm^{-3}{}^{\circ}K^{-1}$	$m^2S^{-1}x10^{-6}$	Mgm^{-3}	$m^3m^{-3}*100$
			4/21/1983		
1	1.6± 0.4	3.06± 0.09	0.5± 0.1	1.38± 0.10	25± 5
2	1.8± 0.7	3.11± 0.13	0.5± 0.2	1.47± 0.09	23± 3
3	1.5± 0.4	3.28± 0.10	0.5± 0.1	1.57± 0.04	23± 2
4	3.9± 1.3	3.25± 0.13	1.2± 0.4	1.71± 0.18	19± 6
			8/24/1983		
1	0.7± 0.5	2.27± 0.16	0.3± 0.2		6± 0
2	1.3± 0.6	2.46± 0.12	0.5± 0.2		7± 0
3	2.1± 1.0	2.60± 0.13	0.8± 0.3		7± 0
4	2.4± 1.1	2.83± 0.29	0.9± 0.4		8± 0

†Layer 1 (0.02-0.06m)
Layer 2 (0.06-0.12m)
Layer 3 (0.12-0.24m)
Layer 4 (0.24-0.44m)

conductivity and heat capacity. In late summer, thermal properties are better correlated with soil density because soil water content is lower and more uniform. These differences, at least in the four layer model, need to be separated for best results. Once the subsurface properties (deeper than 0.024 m) are accounted for (in the four layer model) there proved to be little advantage in further separation of the thermal properties into more layers (Table 2.1, 2.2). The high thermal conductivity and heat capacity in the subsurface (0.24-0.44 m) is due to the high rock fragment content for either time for year. The resultant variability in the values of heat capacity and thermal conductivity, both seasonally and between layers (Table 2.4), indicates the necessity to measure rather than estimate soil density and seasonal water content.

CONCLUSIONS

This project was performed to assess the detail required for measurement of the thermal properties of forest soils in order to better characterize the thermal environment for reforestation sites. The degree of accuracy required, which depends on more specific goals, can dictate the intensity of measurements required. Soil density and water content measurements can be detailed for calculating heat capacities for high resolution of thermal conductivities or averaged over the profile using one measurement for less resolution but simpler field measurements.

Measurements or estimates of soil temperatures are required in combination with heat capacity values. An initial temperature profile is needed for each soil and the boundary conditions must be known or estimated. The lower boundary may be assumed constant but the upper boundary should be measured along with profile measurements. Data from such measurements, in conjunction with the numerical method, can be used to calculate the soil thermal conductivity for a simple "one layer" approach or for more complex multi-layer soils.

There are advantages to using more detailed models, but any of the models predict temperature and heat flux with average accuracy of $\pm 0.4°C$ and ± 0.010 MJ/m^2 respectively. For prediction of maximum and minimum temperatures, four or more soil layers are best. In general, however, all models work equally well in predicting the time of maximum and minimum temperature. For best results in

predicting the duration of temperature above or below some critical level four or more soil layers are also required.

In situations where soils have layers of distinctly different thermal properties use of a model with multiple layers is likely to be quite important. Improvement was shown for our site which was strongly influenced by depth variation of rock fragment content and water content. In profiles with more striking contrast such as soils with surface rock layers or thick organic layers, a layered model would be essential.

REFERENCES

Arnott, J. T.. 1975. Field performance of container-grown and bare-root trees in coastal British Columbia. Can. J. For. Res., 5:186-194

Childs, S. W., H. R. Holbo and E. L. Miller. 1985. Shadecard and shelterwood modification of the soil temperature environment. Soil Sci. Soc. Am. J. 49:1018-1023.

Childs, S. W. and L. E. Flint. 1986. Effect of shadecards, shelterwoods and clearcuts on temperatures and moisture environments. Forest Ecology and Management. Accepted.

de Vries, D. A. 1963. Thermal properties of soils, p. 210-235. In: W. R. Van Wijk (ed.) Physics of plant environment. North-Holland Publishing Co., Amsterdam.

Dobbs R. C. and R. G. McMinn, 1977. Effects of scalping on soil temperature and growth of white spruce seedling. From 6th B. C. Soil Science Workshop Report, April 20-21, 1977, Richmond, B. C.. British Columbia Min. Agr., Victoria.

Firdaouss, M., M. Maalej and B. Belin. 1983. Identification of the soil thermal diffusivity from the temperature in situ measurements in a semi-arid region. In: R. W. Lewis, J. A. Johnson and W. R. Smith (eds.). Proc. 3rd Int'l. Conf. Numerical Methods in Thermal Problems. 2-5 Aug, 1983, Seattle, WA.

Flint, A. L. and S. W. Childs. 1984a. Measuring soil water availability in the field. Forestry Intensified Research Report, 6(2):8-9.

Flint, A. L. and S. W. Childs. 1984b. Physical properties of rock fragments and their effect on available water in skeletal soils. p 91-103. In: Erosion and Productivity of Soils Containing Rock Fragments. Soil Sci. Soc. Amer. Special Pub. No. 13, Soil Sci. Soc. Amer., Madison, WI.

Hallin, W. E. 1968. Soil surface temperatures on cutovers in southwest Oregon. U.S. Forest Service Note, Pacific Northwest Forest and Range Experiment Station, U.S. Department of Agriculture, Portland, OR. April 1968. 17 p.

Hanks, R. J., D. D. Austin, and W. T. Ondrechen. 1971. Soil temperature estimation by a numerical method. Soil Sci. Soc. Am. J. 35:665-667.

Horton, R., P. J. Wierenga and D. R. Nielsen. 1983. Evaluation of methods for determining the apparent thermal diffusivity of soil near the surface. Soil Sci. Soc. Am. J. 47:25-32.

Lopushinsky, W. and M. R. Kaufmann. 1984. Effects of cold soil on water relations and spring growth of Douglas-fir seedlings. Forest Science 30(3):628-634.

Mehuys, G. R., L. H. Stolzy and J. Letey. 1975. Temperature distributions under stones submitted to a diurnal heat wave. Soil Sci. Vol. 120 6:437-441.

Milthorpe, F. L. and J. Moorby. 1974. An introduction to crop physiology. Cambridge University Press. 202 pp.

Parke, J. L., R. G. Linderman and J. M. Trappe. 1983. Effect of root zone temperature on ectomycorrhiza and vesicular-arbuscular mycorrhiza formation in disturbed and undisturbed forest soils of southwest Oregon. Can. J. For. Res. 13:657-665.

Riha. S. J., K. J. McInnes, S. W. Childs, and G. S. Campbell. 1980. A finite element calculation for determining thermal conductivity. Soil Sci. Soc. Am. J. 44:1323-1325

Sorensen, F. C. and R. K. Campbell. 1978. Comparative roles of soil and air temperatures in the timing of spring bud flush in seedling Douglas-fir. Can. J. Bot. 56:2307-2308

van den Driessche, R. 1984. Response of Douglas fir seedlings to phosphorus fertilization and influence of temperature on this response. Plant and Soil 80:155-169.

3. Seasonal Application of a Solar Radiation Model for Mountainous Terrain

Alan L. Flint and Stuart W. Childs

Department of Soil Science

Oregon State University

Seasonal Application of a Solar Radiation Model for Mountainous Terrain[1]

Alan L. Flint and Stuart W. Childs[2]

ABSTRACT

Characteristics of radiation loads on soil-plant systems can be measured or modeled. This study was performed to assess the accuracy with which daily solar radiation can be modeled for horizontal or sloping sites in terrain where surrounding ridges and tall trees block both direct beam and sky diffuse short wave

---

[1]Oregon Agric. Exp. Stn. Technical paper no.____. Contribution of the Dept. of Soil Science, Oregon State Univ., Corvallis, OR. This work was supported as part of the Forestry Intensified Research Program (PNW-80-85), a cooperative project of Oregon State University, the USDA Forest Service, and the USDI Bureau of Land Management.

[2]Graduate Research Assistant and Assistant Professor, Respectively, Dept. of Soil Science, Oregon State University, Corvallis, OR 97331.

radiation. To adequately simulate the major effects on radiation in these environments, the model incorporated 1) standard treatment of solar geometry; 2) separation of direct and diffuse radiation by considering scattering due to aerosols, water vapor, air molecules and ozone; 3) anisotropy of diffuse radiation modeled as a circumsolar component (15 - 50% of the total clear sky diffuse) plus an isotropic background; and 4) proper calculation of the proportions of sky radiation and ground reflected radiation sensed by both horizontal and inclined sensors. The model was calibrated using data from both horizontal and inclined pyranometers at six sites over four years. Values for the Angstrom turbidity coefficient and the percentage of circumsolar diffuse radiation were derived using an iterative best fit technique. Mean monthly values of these coefficients and mean monthly ozone and water vapor concentrations from nearby weather service stations could be used with acceptable accuracy for predicting total, cloud free, daily radiation. Required site measurements include slope, aspect, latitude, longitude, date, time, effective horizon for the site, and an assessment of ground albedo.

INTRODUCTION

The effect of solar radiation on plant growth is known to be a major factor controlling forest site productivity and tree growth. This radiation, the major component of the energy budget for a site, supplies the energy for growth, evaporation, and environmental heating. Solar radiation can be either beneficial and detrimental to plant growth. In situations where plants are growing in close proximity there is competition for photosynthetically active radiation, whereas an excessive radiation load can create conditions of either heat or water stress.

In evaluating reforestation sites, it is common practice to make an assessment of the general environment in which growth must occur after harvest of the existing crop. In most cases, no data are available regarding the radiation environment of a site. Because such information is valuable for estimating the likelihood of excessively harsh environmental conditions, numerous attempts have been made to extrapolate information from nearby measurement sites or to model the receipt of solar radiation. Use of measurements is preferred but is seldom a viable option. On sites where standing timber controls the radiation environment, measurements on the specific site before harvest are not representative of the reforestation environment . Extrapolation of measurements from nearby sites is difficult because site specific factors are, in practice difficult to 1) remove from the original data and 2) estimate for the target site.

Modeling of the radiation environment is an alternative because the cost of obtaining information is relatively low. The success of the modeling approach depends on the quality of the predictions and the availability of the data required to execute the model.

There are techniques available to model radiation which range in accuracy and may be used depending on specific needs. These include calculation of potential direct beam solar radiation without correcting for effects of the atmosphere (e.g. Frank and Lee, 1966; Kaufmann and Weatherred, 1982), calculation of direct and diffuse shortwave radiation components based on simple attenuation models of the atmosphere (e.g. List, 1971; Bristow et al, 1985) and detailed consideration of the nature of scattering in the atmosphere (e.g. Iqbal, 1983; Grant, 1985).

This paper reports on a procedure to calculate solar radiation developed for use in assessing clear sky radiation conditions on reforestation sites in steep, varied terrain. While assessing the utility of various models already available for land managers, it became clear that several important details were not commonly treated. These are:

- Distribution of blocked direct beam radiation on steeply sloping sites with appreciable variation in the horizon due to varied surrounding topography.

- The anisotropic distribution of diffuse radiation and the effects of topographic shading on total diffuse load.

- Ground reflected radiation and intercepted sky radiation when the sky fraction is appreciably less than 2π steradians.

This project was initiated to develop and test a model with sufficient detail to predict radiation delivery to steep sites with irregular horizons. A secondary objective was to minimize the number of field measurements required to operate such a model. We found that detailed consideration of the factors mentioned above was required to accurately predict hourly, daily and seasonal shortwave radiation loads.

MODEL DEVELOPMENT

Proper calculation of total solar radiation load on a specific site requires that three factors be treated:

1. The position of the sun with respect to the location of a specific site on both daily and seasonal time scales.

2. The atmospheric conditions that affect transmission, reflection and scattering of direct beam solar radiation. Treatment of these conditions should allow calculation of the magnitude of diffuse radiation and its distribution in the sky.

3. The physical conditions such as location and orientation of the receiving surface. These are important in calculations of intercepted direct beam, ground reflected radiation and diffuse radiation based on the sky view of sloping sites and the sky view of sensors deployed at a site.

Location of the sun

There are numerous publications that describe the seasonal and daily astronomical relationship between the earth and the sun (e.g. Harris, 1983; List, 1971; U.S.N.O., 1986). We chose to modify a computer program called SUNFINDER (Harris, 1983) which locates the position of the sun in terms of the position on the earth where the sun is directly overhead. This simplifies the sun-earth relationship into a triangle in spherical coordinates with apexes at the site location, the north pole, and the geographical position of the sun. The altitude and azimuth of the sun relative to the earth are calculated by solving the spherical trigonometry problem for the specific latitude, longitude, time of year, time of day and the geographical position of the sun. The SUNFINDER model can be accurately applied to locations between 55°N and 55°S latitudes. The model incorporates the equation of time in order to directly compare modeled radiation with environmental measurements or site observations recorded on a local or clock time basis.

The atmosphere

The intensity of direct beam radiation is reduced and diffuse radiation is increased as the solar beam passes through the atmosphere. Part of the direct beam is reflected at the top of the atmosphere, part is scattered as diffuse radiation, and part is absorbed by the atmosphere. Some models calculate diffuse radiation as a percentage of potential direct beam (Beschta and Weatherred, 1984) or total potential radiation minus actual direct beam (List, 1971; Bristow et al, 1985). These techniques are useful for separating diffuse and direct beam radiation on sloped surfaces but are subject to error if atmospheric conditions change with time. If the solar beam is blocked for significant periods of time by surrounding topography, these simple models can be in error.

There are models that separate measured values of radiation into direct and diffuse components (Weiss and Norman, 1984; Bristow et al 1985) so that components can be applied independently to other nearby sites. The separated direct beam radiation component is corrected to the new slope and the diffuse component is added back. Caution is necessary if the new site has a significantly different surrounding topography which affects diffuse radiation.

The basic form of our treatment of atmospheric effects was taken from the spectrally integrated model of Iqbal (1983). In his work, the reduction in beam radiation and increase in diffuse radiation are modeled as the combined effect of scattering and

absorbance by air molecules and aerosols. Aerosol scatter is calculated from two terms, one related to water vapor concentration and one to account for general atmospheric turbidity (β), as defined by Angstrom's turbidity equation:

$$K_{a\lambda} = \beta \cdot \lambda^{-\alpha} \qquad (3.1)$$

where $K_{a\lambda}$ is the coefficient of attenuation due to scattering and absorption by aerosols, λ is wavelength, α is the wavelength exponent and β is the Angstrom turbidity coefficient. Data from Solmet (1979) allow this wavelength dependent formulation to be used for the entire solar waveband.

Air molecules cause Rayleigh scatter in the atmosphere. The procedure of Iqbal (1983) separates Rayleigh scattering into components of ozone and all other gases. Values for ozone concentration can be obtained from published data (Ozone data for world; Iqbal, 1983). Water vapor concentration data required to assess aerosol scatter can also be obtained from published data (Solmet, 1979) or calculated from regression equations (Iqbal, 1983). The Angstrom turbidity coefficient can be obtained from published data (Solmet, 1979) but can also be obtained from field measurements and the calibration procedures described in the model calibration section. In addition to atmospheric effects, the model of Iqbal also includes a diffuse radiation term to account for secondary scattering of radiation that is reflected from the earth's surface.

Clear sky diffuse radiation is anisotropic in the sky with a large portion near the position of the sun (Figure 3.1). Sky distributions of diffuse radiation have been used with some success by several authors (Stevens, 1977; McArthur and Hay, 1981; Grant, 1985; Klucher, 1979) but there is not general agreement about the proper distribution of radiation, the need for such corrections, and appropriate simplifications for practical application. For our purposes we adopted a simple procedure to model the distribution of diffuse radiation. Because aerosols have a strong forward scatter component, a substantial portion of the aerosol-scattered diffuse radiation appears to come from a small annular area around the sun. We separated this from the other sources so that our model had two components: 1) a circumsolar component of aerosol scattered radiation and 2) an assumed isotropic distribution component due to Rayleigh scattered, ground reflected radiation and the remaining aerosol scatter not attributed to circumsolar radiation. Horizonal brightening was not considered in this simple model of anisotropic

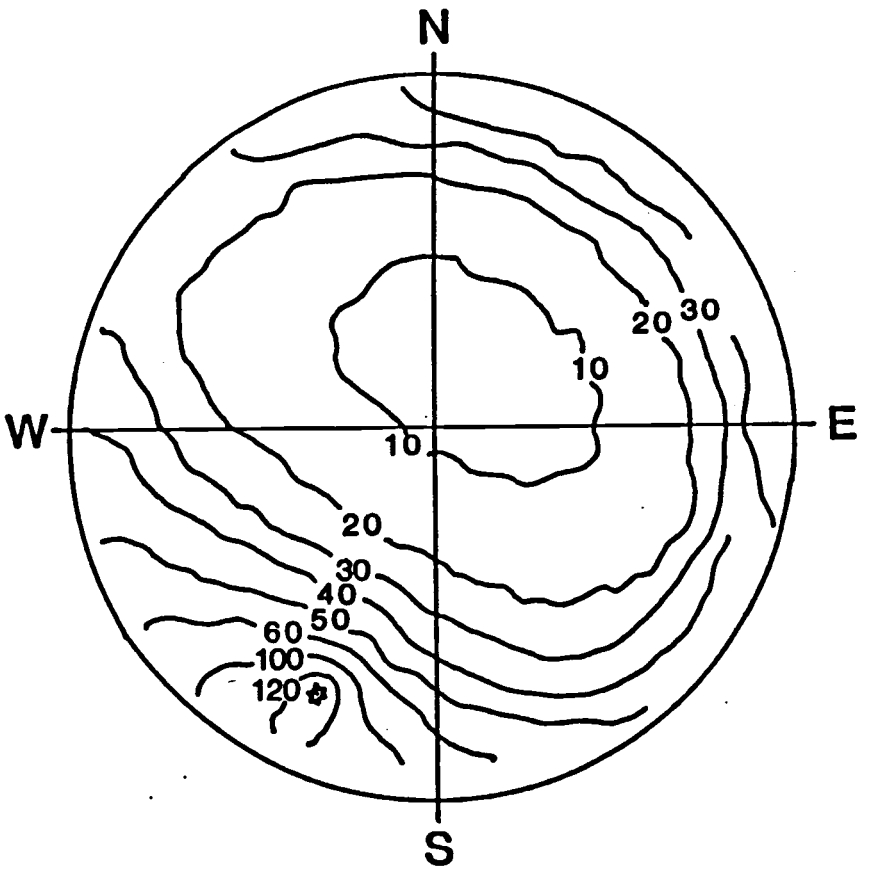

Figure 3.1 Distribution of diffuse radiation under clear sky in $W/m^2/sr$. Solar altitude is 68° and solar azimuth is 194°. Adapted from McArthur and Hay (1981).

diffuse radiation since much of the brightened horizon was blocked by surrounding topography on our study sites.

The receiving surface

Several features of the site must be known or measured. These are latitude, longitude, elevation, slope, aspect, the elevation of surrounding ridges and the albedo of the surrounding area. Latitude and longitude are required to determine solar altitude and azimuth. Longitude is also required to relate solar time to daily time at a specific site. Site elevation is used primarily to determine the thickness of the atmosphere. Slope and aspect are used to calculate the angle of interception of direct beam radiation and also to calculate the proportions of sky hemisphere and surrounding topography which are viewed by the site. For the latter, the effective horizon of a specific site must also be known. Knowledge of the effective horizon is used in order to properly block direct beam, circumsolar diffuse radiation and a percentage of the isotropic diffuse radiation distributed over the sky hemisphere (Figure 3.2). The fraction of sky blocked by the surrounding ridges is used to calculate the effects of these surfaces on radiation flux. The fraction of sky blocked (A_r) was calculated assuming a sky hemisphere of unit radius and using the

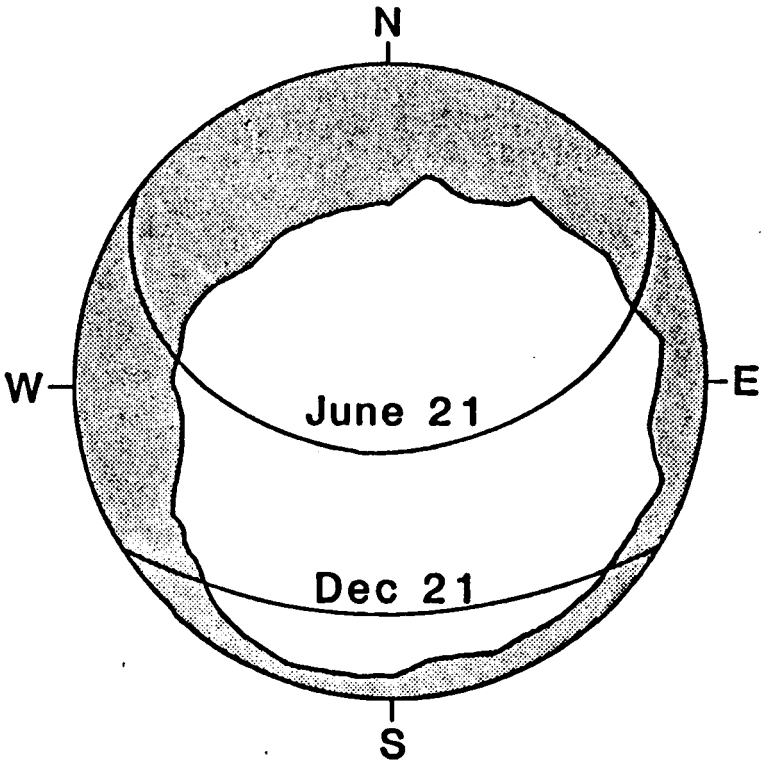

Figure 3.2 View of the sky dome from site at Wolf Creek, Oregon. The solar tracks are for the summer and winter solstice to show topographic blockage (gray area) of direct beam, circumsolar and isotropic sky radiation.

equation for an irregular area on a hemisphere:

$$A_r = \int_{\phi=0}^{2\pi} \int_{\theta=0}^{\theta_r} R^2 \cdot \cos\theta \cdot \partial\theta \cdot \partial\phi / 2\pi \qquad (3.2)$$

where R is the hemisphere radius, θ_r is the altitude of the surrounding ridge and ϕ is aspect. (All symbols are defined in Table 3.2c.) The integral is divided by 2π steradians to scale the surface area to a percentage of the total hemisphere.

Since the altitude of the surrounding ridge (θ_r) is a function of aspect (ϕ), Equation (3.2) is solved by integration with respect to θ and approximation of the integral in ϕ as the summation of 36 0.056π radian increments around the hemisphere:

$$A_r = R^2 \cdot \sum_{n=1}^{36} 0.056\pi \cdot \sin\theta_n \, / 2\pi \qquad (3.3)$$

The overall albedo of the area surrounding a site is required to calculate ground reflected and multiple scattered radiation. This albedo may differ significantly from the specific site albedo used for energy budget calculations. Such a difference is common for forested lands where clearcut areas are surrounded by large areas of forested or well vegetated lands.

MODEL CALIBRATION

The model was calibrated for six different locations (Table 3.1) during four years in southwest Oregon. All measurements were made with Kipp pyranometers (Kipp and Zonen, Delft, Holland) and recorded in digital format using battery powered dataloggers (Model CR-5, Campbell Scientific Inc., Logan, UT in 1980; Model CR-21 in all other years). In 1980, sensors were sampled twice a second and integrated over 15 minutes. At each of these three locations, two pyranometers were used. One was oriented at the same slope and aspect as the site while the other was horizontal. These sites were used to test the model calculation of slope and aspect effects. At the remaining sites, one horizontal pyranometer per site was sampled every 10 seconds and integrated for 30 minutes. These sites were used for seasonal calibration of the model using data for cloud free days.

Location of the sun

The SUNFINDER model (Harris, 1983) calculated sunrise and sunset within 2 minutes time and within 1 degree altitude and azimuth between 55°N and 55°S (as compared with data from U.S.N.O., 1986 and Becker, 1979). Calculation of the sun's location was based on civil time rather than solar time so that comparisons could be conveniently made with other meteorological data measured

Table 3.1. Description of the Study Sites.

Site Designation	Dates of Measurement	Lat (Deg)	Long (Deg)	Aspect (Deg)	Slope (Deg)	Elev. (m)
*Progeny Test	8/ 7/80	42.30	123.65	175	17	564
*Riddle	8/14/80	42.90	123.37	190	15	564
*Turkey Creek	9/11/80	42.87	123.22	165	34	707
Cave Creek	4/81-9/81	42.12	123.48	210	15	1372
Wolf Creek	4/83-3/84	42.72	123.30	191	17	716
Forest Belle	4/84-2/85	42.30	123.10	180	24	1006

*Note: All six sites had radiometers that were horizontal. This site had an additional radiometer oriented with the same slope and aspect as the site.

at the sites. Solar time is based on a daily and seasonally irregular earth-sun relationship whereas clock time is based on an assumed uniform earth-sun relationship. The discrepancy between solar time and clock time is calculated using the equation of time. Since meteorological data are often recorded in terms of local time it is important to correct models or tables of solar radiation from solar time to the same instant or duration of time as the measured data.

The atmosphere

Equations for the atmospheric portion of the model are shown in Table 3.2a, and b. The model was developed by selecting appropriate data for ozone and water vapor, calibrating for the best fit value of Angstrom's turbidity coefficient, and estimating the percentage circumsolar portion of aerosol scattered radiation.

Monthly ozone and water vapor data were used after a sensitivity analysis showed that more detailed treatment was not justified. Monthly average ozone concentrations for 40° W latitude (from Iqbal, 1983) were used for all six sites. Monthly values for the second component, atmospheric precipitable water, were also taken from the literature (Solmet, 1979). There are regression equations available to predict precipitable water from vapor pressure or relative humidity (Iqbal, 1983) but adding this requirement for site data was unwarranted.

The calibration of atmospheric turbidity was simplified by setting the values of ozone and precipitable water to literature values. An iterative technique was then employed to vary the Angstrom turbidity coefficient and compare measured and modeled values to minimize the root mean square error:

$$RMSE = \sum_{i=1}^{N} \left[(Y_i - X_i)^2 / N \right]^{0.5} \qquad (3.4)$$

where Y_i is the i^{th} predicted value, X_i the i^{th} measured value, and N the number of observations over a one day period. Calibrations were made using data for 176 cloud free days from three sites. In order to eliminate error associated with calibration when the sun was near a ridge, calculations were made between 900 and 1500 hours. Two additional statistical tests were used to assess model error. Mean bias error (MBE), the average deviation of predicted values from measured values, was calculated as:

$$MBE = \sum_{i=1}^{N} (Y_i - X_i)/N \qquad (3.5)$$

The model was also evaluated for bias due to time of day or radiation load by calculating RMSE and MBE for three radiation and time classes: sunrise to 900 hours and 1500 hours to sunset; 900 to 1100 hours and 1300 to 1500 hours; and 1100 to 1300 hours (Table 3.3). Daily values were also averaged to monthly values for

comparison with both daily values and published values for the area (data for Medford, OR from Solmet, 1979). These comparisons show a successive reduction in error when more site specific calibration is used. Monthly average values were used in subsequent calibration work because 1) the increase in error over using daily values was small and 2) monthly average values match the resolution used for ozone and water vapor data.

The final step in calibrating the atmospheric portion of the model was estimating the amount of circumsolar radiation and the diameter of the circumsolar disk. This was done using times from the clear sky datasets when the sun was above the theoretical horizon for an infinite planar slope but below the actual horizon determined by surrounding trees and ridges. During these times of only diffuse radiation, the value of measured radiation (also only diffuse) was lower than modeled values for unattenuated diffuse radiation and was attributed to the blocking of circumsolar diffuse radiation by the ridge. The aerosol scattered diffuse radiation predicted by the model was iteratively reduced to match measured diffuse radiation data. The best fit of model to measurements was assessed using RMSE (Eq. 3.4). Generally one quarter to three quarters of the aerosol scattered radiation was calculated as circumsolar (Table 3.4). The results were, for model simplicity, averaged on a monthly basis for the three long term sites to match the monthly values of ozone, precipitable water and atmospheric turbidity (Table 3.4).

The evaluation of circumsolar radiation showed little difference between morning and evening for any date or any site though there were significant changes seasonally. It is not known if these values remain constant at midday when the solar pathlength through the atmosphere is shortest, however, it is assumed constant in this model. Reducing the aerosol scattered diffuse radiation could not be simply applied when the sun was behind the ridge but needed to be applied when the sun was within 4 degrees of the ridge. From Figure 3.1 it can be seen that a significant portion of the diffuse radiation would be blocked even before the sun would be behind a ridge. Figure 3.3c shows the modeled reduction of diffuse radiation at least 30 minutes before the sun was behind the ridge.

The receiving surface

The receiving surface parameters vary between sites with the main seasonal effect being albedo since all other parameters are fixed with time. The model was tested against measured data taken by a horizontal Kipp radiometer. Although all parameters on the six sites vary (Table 3.1), factors of slope and aspect do not affect the horizontal radiometers. The three sloping Kipp radiometers located on the short term sites indicated in Table 3.1, were used to evaluate the ability of the calibrated model to predict the radiation environment on the sloping surface.

The series of steps to model the radiation for a site radiation is represented in Figures 3.3a, 3.3b, and 3.3c. This series shows the major changes needed to correctly account for surrounding topography. In Figure 3.3a the atmospheric portion of the model has been calibrated to match the midday radiation (0900 hours to 1500 hours) but does not match the early and late portions of the day. In Figure 3.3b the surrounding topography, previously incorporated in the calculation of ground reflected radiation, is now used to block direct beam radiation leaving only diffuse radiation early and late in the day. Agreement between the model and measurements is much better. Finally, Figure 3.3c incorporates the blockage of circumsolar diffuse radiation. Although this series of graphs is a simplification of the actual procedure, this series adequately describes the method of evaluation in mountainous terrain.

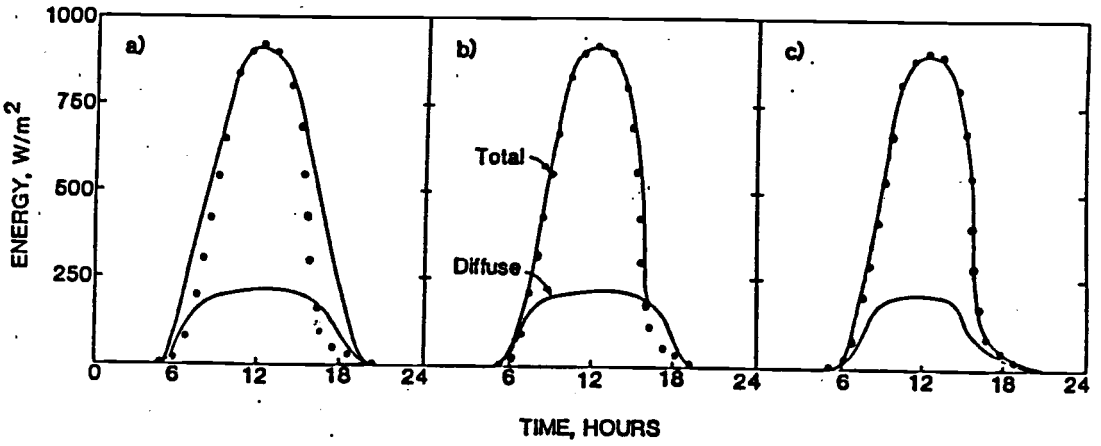

Figure 3.3a, b, and c. Measured shortwave radiation (•) with modeled diffuse and direct beam radiation: (a) without incorporation of surrounding topography, (b) incorporation of surrounding topography to block only direct beam radiation and (c) incorporation of surrounding topography to block both direct beam radiation and circumsolar diffuse radiation. The data are for Wolf Creek, Oregon, August 6, 1983.

Table 3.2a. Radiation model for direct and diffuse radiation. The model is primarily that of Iqbal (1983).

DIRECT BEAM: $I_n = 0.9751 \cdot I_{sc} \cdot \gamma_r \cdot \gamma_o \cdot \gamma_g \cdot \gamma_w \cdot \gamma_a$

$I_{sc} = 1367\ W/m^2$

$0.9751 =$ constant required to treat 0.3-3.0 μm wavelengths

$\gamma_r = \exp[-0.0903 \cdot M_a^{0.84} \cdot (1.04+M_a-M_a^{1.01})]$

$\gamma_o = 1 - [0.1611 \cdot U_3 \cdot (1.0+139.48 \cdot U_3)^{-0.3035}$

$- 0.002715 \cdot U_3 \cdot (1.0+0.044 \cdot U_3+0.0003 \cdot U_3)^{-1}]$

$\gamma_g = \exp(-0.0127 \cdot Ma^{.26})$

$\gamma_w = 1 - 2.4959KU_1[(1.0+79.034 \cdot U_1)^{0.6828}+6.385 \cdot U_1]^{-1}$

$\gamma_a = (0.12445 \cdot \alpha-0.0162)+(1.003-.125 \cdot a)$

$\exp[-\beta M_a(1.089 \cdot \alpha+0.5123)],\ \beta < 0.5$

$U_1 = W \cdot M_r$

$U_3 = L \cdot M_r$

$M_r = [\cos\theta_z+0.15(93.885-\theta_z)^{-1.253}]^{-1}$

$M_a = M_r(P/1013.25)$

$P/P_o = \exp(-0.0001184 \cdot Z)$

Table 3.2a (continued)

DIFFUSE RADIATION: $I_d = I_{dr}+I_{da}+I_{dm}$

$$I_{dr} = 0.79 \cdot I_{sc} \cdot \cos\theta_z \cdot \gamma_o \cdot \gamma_g \cdot \gamma_w \cdot \gamma_{aa} \cdot \gamma 0.5(1-\gamma_r)/(1-M_a+M_a^{1.02})$$

$$\gamma_{aa} = 1-(1-W_o)(1-M_a+M_a^{1.06})(1-\gamma_a),\ W_o=0.9$$

$$I_{da} = 0.79 \cdot I_{sc} \cdot \cos\theta_z \cdot \gamma_o \cdot \gamma_g \cdot \gamma_w \cdot \gamma_{aa} \cdot Fc(1-\gamma_{as})/(1-M_a+M_a^{1.02})$$

$$\gamma_{as} = \gamma_a/\gamma_{aa},\ Fc=0.84$$

$$I_{dm} = (I_n \cdot \cos\theta_z+I_{dr}+I_{da})P_g \cdot P_a/(1-P_g \cdot P_a)$$

$$P_a = 0.0685+(1-Fc)(1-\gamma_{as})$$

TOTAL RADIATION FOR PLANAR SURFACE: $I = I_n \cdot \cos\theta_z+I_d$

GROUND REFLECTED RADIATION

$$I_r = I \cdot P_g \cdot A_r$$

$$I_s = (I_d-CSR) \cdot A_s+CSR$$

TOTAL RADIATION RECEIVED BY SURFACE: $I_t = I_n \cdot \cos\theta_z+I_s+I_r$

Table 3.2b. Definition of symbols.

A_r	Percentage ground area projected on sky dome
A_s	Percentage sky area projected on sky dome ($1-A_r$)
CSR	Circumsolar radiation (W/m^2)
Fc	Fraction of forward scatter to total scatter (dimensionless)
I	Total Radiation incident on a surface ((W/m^2)
I_d	Total diffuse irradiance on a horizontal surface (W/m^2)
I_{da}	Aerosol scattered radiation (W/m^2)
I_{dm}	Multiple reflected radiation (W/m^2)
I_{dr}	Rayleigh scattered radiation (W/m^2)
I_n	Direct normal irradiance (W/m^2)
I_r	Ground reflected diffuse radiation incident on an inclined surface (W/m^2)
I_s	Sky diffuse radiation incident on an inclined surface (W/m^2)
I_{sc}	Solar Constant (1367 W/m^2)
L	Thickness of ozone layer (cm)
M_a	Air mass at actual pressure (dimensionless)
M_r	Air mass at standard pressure 1013.25 mbars (dimensionless)
P	Atmospheric pressure (mbars)
P_o	Standard atmospheric pressure 1013.25 mbars
U_1	Total pressure-corrected relative optical path length for water vapor (cm)
U_3	Total optical path length for ozone [cm(NTP)]
W	Precipitable water (cm)

Table 3.2b (continued)

W_o Fraction of energy scattered to attenuation by aerosols (dimensionless)

Z Altitude of site (m)

α_o Fraction of incident radiation absorbed by ozone (dimensionless)

α_w Fraction of incident radiation absorbed by water (dimensionless)

β Angstrom's turbidity parameter (dimensionless)

θ_z Zenith angle of the sun with respect to the vertical (deg)

γ_r Fraction of incident radiation transmitted by air molecules (dimensionless)

γ_o Fraction of incident radiation transmitted by ozone (dimensionless)

γ_g Fraction of incident radiation transmitted after absorption by mixed gases (dimensionless)

γ_w Fraction of incident radiation transmitted by water vapor (dimensionless)

γ_a Fraction of incident radiation transmitted by aerosols (dimensionless)

γ_{aa} Fraction of incident radiation transmitted after absorption by aerosols (dimensionless)

γ_{as} Fraction of incident energy transmitted after scatter by aerosols (dimensionless)

P_a Albedo of cloudless-sky atmosphere (dimensionless)

P_g Albedo of ground or ground cover (dimensionless)

RESULTS AND DISCUSSION

The results will be discussed in four parts, 1) the magnitude of the direct, diffuse and ground reflected radiation, 2) the sensitivity of the model to variation of atmospheric turbidity, ozone and precipitable water, 3) the effect of slope, aspect and surrounding ridges on radiation and 4) model sensitivity to use of monthly averages values of atmospheric turbidity.

Magnitudes of various components. The monthly contribution of each radiation component is shown in Figure 3.4 and the range of environmental conditions is summarized in Table 3.4. Multiple scatter radiation (the radiation scattered after reflection from the ground surface) averages 2 percent with larger values (4 percent) in winter when ground albedo is the highest, largely due to snow. Rayleigh scatter radiation is the next smallest value, averaging about 4 percent throughout the year. Ground reflected radiation averages 8 percent with a larger contribution (15 percent) in winter when ground albedo is the highest. Aerosol scattering provides the largest diffuse radiation component (14 percent average) and 25 to 75 percent of that total was circumsolar (Table 3.4). Circumsolar radiation therefore comprised about 7 percent of the total radiation. Total diffuse radiation averaged about 20 percent of the total radiation for clear sky conditions. Although direct beam radiation is the major component it only contributes about half of the total

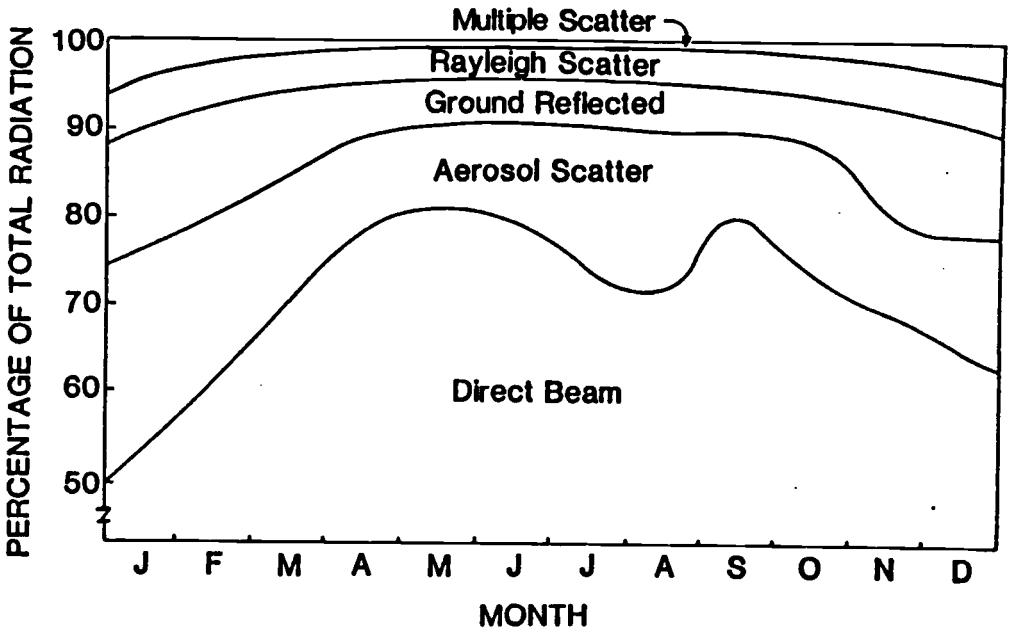

Figure 3.4 Seasonal contribution of radiation components: direct beam, aerosol scattered diffuse, Rayleigh scattered diffuse, multiple scatter diffuse, and ground reflected radiation.

Table 3.3. Error in radiation model for root mean square error (RMSE) and mean bias error (MBE) for all clear sky days at three sites. The data are mean plus or minus one standard deviation. The low radiation class is from sunrise to 900 hours and 1500 hours to sunset, medium radiation is from 900 hours to 1100 hours and 1300 hours to 1500 hours and high radiation is 1100 to 1300 hours. The data were analyzed using the best daily value of β, the monthly average of β, and the monthly average values of β obtained from Solmet (1979).

	Radiation Load Class				
	Low	Medium	High	All Day	Source of β value
Wolf Creek					
RMSE	42±12	5±4	13±5	33±9	Daily
MBE	10±9	1±4	0±2	6±5	
RMSE	42±12	12±8	18±7	34±9	Monthly
MBE	10±10	1±14	0±12	6±9	
RMSE	41±9	37±24	38±20	41±11	Solmet
MBE	-1±14	-29±33	-28±30	-13±20	
Forest Belle					
RMSE	31±13	5±6	9±10	24±11	Daily
MBE	1±9	0±6	-1±4	1±5	
RMSE	32±13	11±7	14±10	26±11	Monthly
MBE	2±11	1±1	-1±11	1±9	
RMSE	38±12	43±25	42±23	41±17	Solmet
MBE	-20±12	-43±26	-41±25	-29±17	
Cave Creek					
RMSE	81±31	7±6	23±14	65±25	Daily
MBE	10±12	0±6	0±3	6±7	
RMSE	82±31	16±11	28±14	66±24	Monthly
MBE	10±13	-1±18	-1±16	5±13	
RMSE	81±25	44±23	49±20	71±20	Solmet
MBE	-6±14	-43±24	-40±21	-20±16	

Table 3.4. Atmospheric inputs by month for Wolf Creek. The inputs are atmospheric turbidity (β), precipitable water (PW), ozone, circumsolar radiation (CSR), and ground albedo. Data used are from Solmet (1979) or were calculated during calibration for the site.

Month	β		PW (cm)	Ozone (cm)	CSR (%)	Ground Albedo
	Site	Solmet	Solmet	Iqbal	Site	Solmet
January	0.16	(0.09)	1.13	0.30	25	0.496
February	0.15	(0.13)	1.02	0.32	25	0.400
March	0.12	(0.16)	0.97	0.33	25	0.313
April	0.10	(0.19)	1.00	0.34	25	0.192
May	0.09	(0.22)	1.30	0.34	50	0.140
June	0.11	(0.20)	1.59	0.33	50	0.140
July	0.17	(0.17)	1.64	0.31	75	0.140
August	0.19	(0.17)	1.65	0.30	75	0.140
September	0.08	(0.22)	1.43	0.28	50	0.140
October	0.11	(0.20)	1.27	0.27	50	0.192
November	0.08	(0.15)	1.30	0.28	25	0.365
December	0.08	(0.09)	1.06	0.29	25	0.418

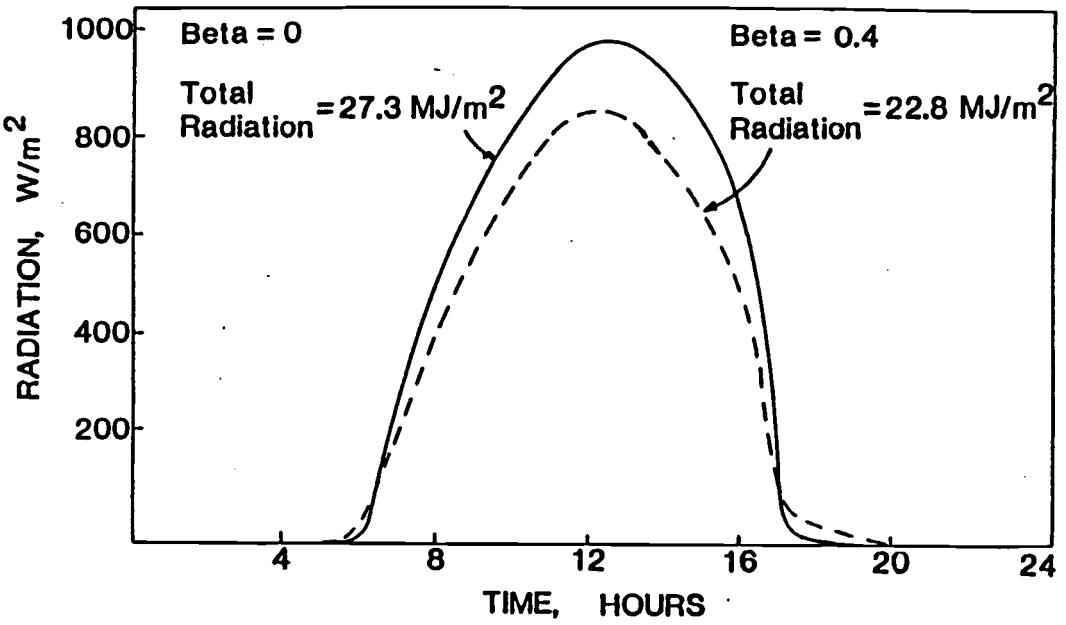

Figure 3.5 Effect of changing atmospheric turbidity between β = 0.0 and 0.4. Note the crossover of radiation when the direct beam is blocked by the surrounding topography. This occurs because higher atmospheric turbidity increases the amount of diffuse radiation.

radiation in January when aerosol scattered and ground reflected radiation components are large.

The sensitivity of the model to different values of turbidity is shown in Figure 3.5. Increasing values from 0.0 to 0.4 reduced peak radiation from 922 to 818 W/m^2 and reduced total radiation by 4.5 MJ/m^2/day. The commonly encountered range of atmospheric turbidity includes $\beta = 0.0$ (clean air), $\beta = 0.1$ (clear air), $\beta = 0.3$ (turbid air) and $\beta = 0.4$ (very turbid air). With increasing turbidity, total radiation is reduced but the contribution of diffuse increases. This can be seen at the crossover points (Figure 3.5) when the sun goes behind the ridge and the larger diffuse radiation component when $\beta = 0.4$ becomes apparent.

Sensitivity of the model. A more complete analysis of the parameters of atmospheric turbidity, precipitable water and ozone is presented in Table 3.5. These parameters were varied over a reasonable range to determine the effect on model output of peak radiation and total radiation over the day. As demonstrated in Figure 3.5, atmospheric turbidity has the largest influence. Precipitable water is also important because total daily radiation would be overestimated by more than 3 MJ/m^2 if it were assumed zero. Ozone concentration has little influence on total radiation since it is mostly scattering small wave length radiation (Rayleigh scatter). Although elimination of the ozone term would not greatly affect accuracy, literature values are easily found. Calibration

for this parameter is unnecessary so there is no advantage in simplifying the model.

Effect of slope, aspect and topography. These is little effect of slope, aspect and surrounding topography on the accuracy of model predictions. The three sites shown in Table 3.3 have similar time of day bias even though their orientations are different. The largest error in calculating radiation occurs during the period of low radiation intensity, that period corresponding to the time of sun-ridge interaction. The larger errors found in the Cave Creek data set are due to a lack of information about the surrounding topography. The surrounding forest land was clearcut after radiation measurements were made and before data were taken to determine the position of trees that would block the sun. Partial reconstruction was successful and provided enough information to use the data set.

After the model was calibrated for three sites using data from horizontal pyranometers, data from sloping radiometers were used to validate the model correction for slope, aspect, and topographic view factor. The daily variation in radiation between a sloping surface and a horizontal surface is well represented by the model for the Turkey Creek site (Figure 3.6.).

Daily variation in radiation between a sloping surface and a horizontal surface was modeled over an entire season assuming all days to be cloudless. This seasonally modeled radiation on a

Table 3.5. Sensitivity to changes in atmospheric turbidity (β), precipitable water (PW) and ozone. Data for the Wolf Creek site, August 6, 1983.

β	PW	Ozone	Radiation		Effect of
			Peak	Total	
	(cm)	(cm)	W/m^2	$MJ/m^2/day$	
0.00	1.65	0.30	991	28.1	
0.10	1.65	0.30	944	26.5	
→0.19	1.65	0.30	907	25.3	β
0.20	1.65	0.30	903	25.2	
0.30	1.65	0.30	869	24.2	
0.40	1.65	0.30	840	23.3	
0.19	0.00	0.30	1019	28.5	
0.19	1.00	0.30	919	25.7	
→0.19	1.65	0.30	907	25.3	PW
0.19	2.00	0.30	902	25.2	
0.19	3.00	0.30	891	24.9	
0.19	1.65	0.00	922	25.8	
0.19	1.65	0.10	915	25.6	
0.19	1.65	0.20	911	25.4	Ozone
→0.19	1.65	0.30	907	25.3	
0.19	1.65	0.40	904	25.2	

→Actual conditions for the site.

horizontal surface and the sloping surface for Wolf Creek is significantly different (Figure 3.7). The sloping surface receives significantly more radiation over the year except for mid summer, near the solstice when the sun has approximately the same zenith angle on both the horizontal surface and the 17° sloping surface. The irregularity of the seasonal radiation curve is largely due to the changing environmental condition of atmospheric turbidity.

Use of average monthly turbidity values. The high and medium radiation intensity classes for all sites were within 30 W/m2 RMSE and 1 W/m2 MBE when daily or monthly turbidity values were used (Table 3.3). When Solmet values were used, RMSE was between 40 and 50 W/m2. The error was due mainly to the large MBE which was nearly the same value as the RMSE, indicating a simple bias error due to an overestimate of atmospheric turbidity (Table 3.3). The Solmet data are for Medford, Oregon, an urban/industrial area where atmospheric turbidity is expected to be higher than in the nearby coast range where our sites were located.

Model errors assessed by RMSE, MBE and time of day bias indicate that use of monthly average turbidity for a site is an acceptable substitute for daily values (Table 3.3). Monthly turbidity values are at the same level of detail as the monthly values of ozone, precipitable water and circumsolar radiation used in the model. Literature values of turbidity are not, however, acceptable except for initial analysis of prospective sites.

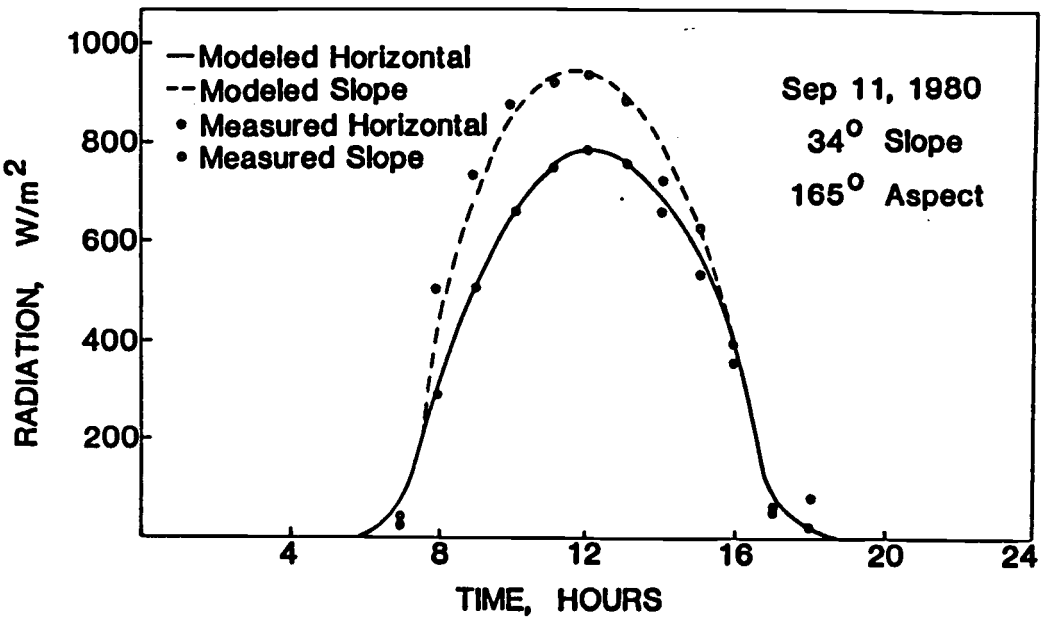

Figure 3.6 Measured and modeled diurnal radiation at Turkey Creek, Oregon for horizontal (•) and sloping (○) radiometers.

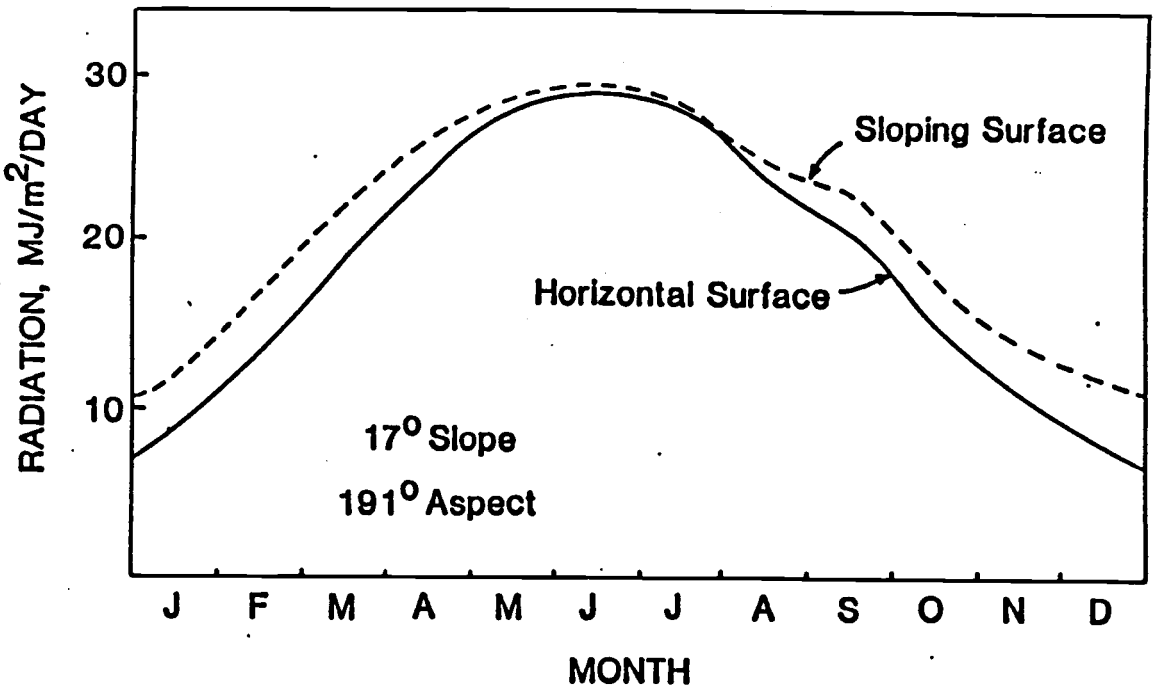

Figure 3.7 Seasonal variation in total daily radiation on a horizontal surface and a sloping surface for Wolf Creek, Oregon.

CONCLUSIONS

This model is a simple, effective way to predict radiation received by a specific site in mountainous terrain. The site specific parameters required for input are basic and simple to acquire. The atmospheric parameters of ozone and precipitable water are insensitive enough so that literature values (Solmet, 1979; Iqbal, 1983) may be used. Atmospheric turbidity can be estimated from visibility data (Iqbal, 1983) or taken from measurements at or nearby the site.

Perhaps the most significant detail determining the accuracy of the model is the nature of the surrounding topography and the slope and aspect of the receiving surface. Although this model was calibrated for mountainous terrain it is also useable on any other topographic setting, such as large flat or sloping agricultural areas.

Data from measuring stations can be used to calibrate the model for specific days or longer periods of time. Once calibrated, the model can be used for a variety of site specific environments where slope, aspect, albedo and surrounding topographic conditions are known. Since the calibration of atmospheric turbidity is fairly robust, application of the model can be made some distance from the measuring station if atmospheric conditions are expected to be similar.

REFERENCES

Becker, C. F. 1979. Solar radiation availability on surfaces in the united states as affected by season, orientation, latitude, altitude and cloudiness. Arno Press, New York. 107pp.

Beschta, R. L. and J. Weatherred. 1984. TEMP-84: A computer model for predicting stream temperatures resulting from the management of streamside vegetation. WSDG Report WSDG-AD-00009, July. USDA Forest Service, Watershed Systems Development Group, Fort Collins, Colorado.

Bristow, K. L., Campbell, G. S. and Saxton, K. E. 1985. An equation for separating daily solar irradiation into direct and diffuse components. Agric. For. Meteorol., 35:123-131

Frank, E C., and R. Lee. 1966. Potential solar beam radiation on slopes: Tables for 30° and 50° latitude. USDA Forest Service Research Paper RM-18, 116p. Rocky Mountain Forest and Range Experiment Station, Fort Collins, Colo.

Grant, R. H. 1985. The influence of the sky radiance distribution on the flux density in the shadow of a tree crown. Agric. For. Meteorol., 35:59-70

Harris, S. 1983. Catching rays. 80 Micro. October. p 256-262.

Iqbal, M. 1983. An introduction to solar radiation. Academic Press. 309pp.

Kaufmann, M. R. and J. D. Weatherred, 1982. Determination of potential direct beam solar irradiance. USDA Forest Service Research Paper RM-242. Rocky Mountain Forest and Range Experiment Station, Fort Collins, Colo.

Klucher, T. M., 1979. Evaluation of models to predict insolation on tilted surfaces. Solar Energy 23(2), 111-114.

List, R. J. 1971. Smithsonian meteorological tables. 527 p. Smithsonian Institution Press, Washington, D.C.

McArthur, L. J. B. and J. E. Hay. 1981. A technique for mapping the distribution of diffuse solar radiation over the sky hemisphere. Journal of Applied Meteorology, 20:421-429.

Ozone data for the world. Meteorological Service for Canada, Issued Monthly.

Solmet Vol. 2. (1979). Hourly solar radiation-surface meteorological observations. Final Report TD-9724. National Climatic Center, Asheville, North Carolina.

Stevens, M. D. 1977. Standard distributions of clear sky radiance. Quart. J. Roy. Meteor. Soc., 103:457-465.

U.S.N.O. United States Naval Observatory; 1986. The Astronomical Almanac, U. S. Government Printing Office, Washington D. D..

Weiss, A. and Norman, J.M. 1984. Partitioning solar radiation into direct and diffuse, visible and near-infrared components. Agric. For. Meteorol., 34:205-213.

SUMMARY

The three models presented in this thesis can be used together or independently for a variety of purposes. The energy balance framework (Eq. 1) suggests ways in which these models can be used to evaluate reforestation sites and environmental conditions after harvesting. This summary will be used to address the direction further research should go that best incorporates measurements and models.

The surface energy balance can be used to estimate potentials for heating and evaporation on reforestation sites, particularly at the soil-atmosphere interface. Potential soil surface temperatures can be solved by estimating or modeling all other parameters in the energy balance equation (Eq. 1) and solving the net radiation term (Q^*) for the longwave emitted (Eq. 1.6) from the soil surface, which is a function of surface temperature. This technique can be used to solve for any one unknown if all the other terms in the equation are assigned some value, either measured or estimated. The disadvantage to this technique is that some of the components, particularly sensible heat flux, are hard to model or estimate.

The solar radiation model can be used to determine potential radiation on a variety of sites. The radiation model will give magnitudes of potential solar radiation as well as the timing for those magnitudes. By matching reforestation field experience on these sites with modeled potential radiation, a practical range of data would be available to evaluate future sites. The field

experience should incorporate calculations of the potential radiation environment with a knowledge of soil types where failures have occurred to predict future problems on similar sites. Information on soil types may be reduced to a simple estimate or measurement of soil properties, such as rock fragment content and water content.

A major area for application of the models is in determining the influence of soil temperature on seedling establishment. Once soil thermal properties for a particular site are known or calculated, then a range of possible surface temperatures can be used with the soil heat flow equation to determine the amount and depth of absorption of energy in the profile or the likelihood of critical soil temperatures near the surface. This technique can be used to determine the duration of specific soil temperature conditions and the possibility of adverse impacts on plant roots and soil fungi.

The potential effects of various soil management strategies, such as mulching, could be assessed by application of the models. The soil surface conditions can be changed by adding to a model some surface mulching condition and then determine if the new condition would ameliorate the subsurface temperatures. It is both the duration and the absolute temperature values which are important to seedling survival. The actual values are still needed and may only be determined by case studies or laboratory techniques. Once determined the conditions in the field which

would lead to these temperatures can be evaluated by using the models.

Another major consideration in reforestation is loss of soil water. The advantage of using the Priestley-Taylor equation for solving for latent heat flux and therefore evaporation is that sensible heat flux is not required. The Priestley-Taylor formulation requires net radiation, a function of air temperature, soil surface temperature, solar radiation, and ground heat flux which is dependent on soil temperatures and soil thermal properties. These terms can be estimated using the measurement and modeling techniques presented in the thesis. With this formulation we eliminate the need to measure or estimate of sensible heat flux, at least to determine evaporation losses.

This evaporation model can be used with measured environmental conditions to estimate available soil water or determine the timing of soil water loss. Evaporation from the soil surface and plant transpiration are the major components in the water budget and can be used to suggest if water conservation procedures are needed, such as using mulchs, shelterwoods, or hardier seedlings which can better withstand possible moisture stress conditions. Field experience can be combined with models such as this one to determine the appropriate amount of soil moisture needed for successful regeneration.

The combination of all models could provide a method to examine different principles involved in reforestation microclimate. The solar radiation model can be used with

measurements or estimates of soil and air temperature to calculate potential net radiation. The modeled values of net radiation and an estimate of soil heat flux can be incorporated into the Priestley-Taylor model to simulate environmental conditions of heat and moisture stress for a reforestation site. An example would be a sensitivity analysis to determine the influence of changing environmental conditions such as atmospheric turbidity, mulched surface or vegetative water use.

In the final analysis, these models can be applied to areas where actual field experience can provide a test to determine the critical conditions that lead to reforestation failures. Models are only a beginning to solve the reforestation problems in southwest Oregon but with wide field application by experienced field workers these models can incorporate specific field knowledge and help determine the range of conditions which encompass successful and unsuccessful reforestation. Once this range is known these models can be applied to determine possible future problems. The models can also be used to teach field workers the conceptual framework in which to store and evaluate field measurements or observations. It will take an integrated approach to measurements and modeling to find a final solution by interested and dedicated land managers and researchers.

BIBLIOGRAPHY

Arnott, J. T.. 1975. Field performance of container-grown and bare-root trees in coastal British Columbia. Can. J. For. Res., 5:186-194

Barton, I. J., 1979. A parameterization of the evaporation from nonsaturated surfaces. Journal of Applied Meteorology. 18:43-47.

Becker, C. F. 1979. Solar radiation availability on surfaces in the united states as affected by season, orientation, latitude, altitude and cloudiness. Arno Press, New York. 107pp.

Beschta, R. L. and J. Weatherred. 1984. TEMP-84: A computer model for predicting stream temperatures resulting from the management of streamside vegetation. WSDG Report WSDG-AD-00009, July. USDA Forest Service, Watershed Systems Development Group, Fort Collins, Colorado.

Black T. A., 1979. Evapotranspiration from Douglas-fir stands exposed to soil water deficits. Water Resources Research. 15(1):164-170.

Black, T. A. and D. L. Spittlehouse. 1980. Modeling the water balance for watershed management. p. 117-129. In: D. M. Baumgartner, (Ed.), Interior West Watershed Management. Washington State University. Pullman, Washington.

Bristow, K. L., Campbell, G. S. and Saxton, K. E. 1985. An equation for separating daily solar irradiation into direct and diffuse components. Agric. For. Meteorol., 35:123-131

Campbell, G. S., 1977 An Introduction to Environmental Biophysics Springer-Verlag, New York, 159 pp.

Childs, S. W., H. R. Holbo and E. L. Miller. 1985. Shadecard and shelterwood modification of the soil temperature environment. Soil Sci. Soc. Am. J. 49:1018-1023.

Childs, S. W. and L. E. Flint. 1986. Effect of shadecards, shelterwoods and clearcuts on temperatures and moisture environments. Forest Ecology and Management. Accepted.

Davies J. A. and C. D. Allen, 1973. Equilibrium, potential and actual evaporation from cropped surfaces in southern Ontario. Journal of Applied Meteorology. 12:649-657.

De Bruin H. A. R. 1983. A model for the Priestley-Taylor parameter α. Journal of Climate and Applied Meteorology. 22:572-578.

De Bruin, H. A. R., and A. A. M. Holtslag, 1982. A simple parameterization of the surface fluxes of sensible and latent heat during daytime compared with the Penman-Monteith concept. Journal of Applied Meteorology. 21:1610-1621.

Denmead, O. T., and R. J. Shaw. 1962. Availability of soil water to plants as affected by soil moisture content and meteorological conditions. Agron. J. 54:385-390.

de Vries, D. A. 1963. Thermal properties of soils, p. 210-235. In: W. R. Van Wijk (ed.) Physics of plant environment. North-Holland Publishing Co., Amsterdam.

Dobbs R. C. and R. G. McMinn, 1977. Effects of scalping on soil temperature and growth of white spruce seedling. From 6th B. C. Soil Science Workshop Report, April 20-21, 1977, Richmond, B. C.. British Columbia Min. Agr., Victoria.

Firdaouss, M., M. Maalej and B. Belin. 1983. Identification of the soil thermal diffusivity from the temperature in situ measurements in a semi-arid region. In: R. W. Lewis, J. A. Johnson and W. R. Smith (eds.). Proc. 3rd Int'l. Conf. Numerical Methods in Thermal Problems. 2-5 Aug, 1983, Seattle, WA.

Flint, A. L. and S. W. Childs. 1984a. Measuring soil water availability in the field. Forestry Intensified Research Report, 6(2):8-9.

Flint, A. L. and S. W. Childs. 1984b. Physical properties of rock fragments and their effect on available water in skeletal soils. p. 91-103. In: Erosion and Productivity of Soils Containing Rock Fragments. Soil Sci. Soc. Amer. Special Pub. No. 13, Soil Sci. Soc. Amer., Madison, WI.

Frank, E C., and R. Lee. 1966. Potential solar beam radiation on slopes: Tables for 30° and 50° latitude. USDA Forest Service Research Paper RM-18, 116p. Rocky Mountain Forest and Range Experiment Station, Fort Collins, Colo.

Giles, D. G., T. A. Black, and D. L. Spittlehouse. 1985. Determination of growing season soil water deficits on a forested slope using water balance analysis. Can. J. For. Res. 15:107-114.

Grant, R. H. 1985. The influence of the sky radiance distribution on the flux density in the shadow of a tree crown. Agric. For. Meteorol., 35:59-70

Hallin, W. E. 1968. Soil surface temperatures on cutovers in southwest Oregon. U.S. Forest Service Note, Pacific Northwest Forest and Range Experiment Station, U.S. Department of Agriculture, Portland, OR. April 1968. 17 p.

Hanks, R. J., D. D. Austin, and W. T. Ondrechen. 1971. Soil temperature estimation by a numerical method. Soil Sci. Soc. Am. J. 35:665-667.

Harris, S. 1983. Catching rays. 80 Micro. October. p 256-262.

Holbo, H. R., 1981. A dew-point hygrometer for field use. Agric. Meteorol. 24:117-130.

Holbo, H. R., S. W. Childs, and E. L. Miller. 1986 Summertime radiation balances of clearcuts and shelterwood slopes in southwest Oregon. Forest Science. Submitted.

Horton, R., P. J. Wierenga and D. R. Nielsen. 1983. Evaluation of methods for determining the apparent thermal diffusivity of soil near the surface. Soil Sci. Soc. Am. J. 47:25-32.

Iqbal, M. 1983. An introduction to solar radiation. Academic Press. 309pp.

Jury, W. A. and C. B. Tanner. 1975. Advection modification of the Priestley and Taylor evapotranspiration formula. Agronomy Journal 67:840-842.

Kaufmann, M. R. and J. D. Weatherred, 1982. Determination of potential direct beam solar irradiance. USDA Forest Service Research Paper RM-242. Rocky Mountain Forest and Range Experiment Station, Fort Collins, Colo.

Klucher, T. M., 1979. Evaluation of models to predict insolation on tilted surfaces. Solar Energy 23(2), 111-114.

List, R. J. 1971. Smithsonian meteorological tables. 527 p. Smithsonian Institution Press, Washington, D.C.

Lopushinsky, W. and M. R. Kaufmann. 1984. Effects of cold soil on water relations and spring growth of Douglas-fir seedlings. Forest Science 30(3):628-634.

McArthur, L. J. B. and J. E. Hay. 1981. A technique for mapping the distribution of diffuse solar radiation over the sky hemisphere. Journal of Applied Meteorology, 20:421-429.

McNaughton, K. G., and T. A. Black, 1973. A study of evapotranspiration from a Douglas-fir forest using the energy balance approach. Water Resources Research. 9:1579-1590.

Mehuys, G. R., L. H. Stolzy and J. Letey. 1975. Temperature distributions under stones submitted to a diurnal heat wave. Soil Sci. Vol. 120 6:437-441.

Milthorpe, F. L. and J. Moorby. 1974. An introduction to crop physiology. Cambridge University Press. 202 pp.

Monteith, J. L. 1964. Evaporation and environment. In The Stat and Movement of Water in Living Organisms. 19th Symp. Soc. exp. Biol., 205.

Mukammal, E. I. and H. H. Neumann, 1977. Application of the Priestley-Taylor evaporation model to assess the influence of soil moisture on the evaporation from a large weighing lysimeter and class A pan. Boundary Layer Meteorology. 12:243-256.

Ozone data for the world. Meteorological Service for Canada, Issued Monthly.

Parke, J. L., R. G. Linderman and J. M. Trappe. 1983. Effect of root zone temperature on ectomycorrhiza and vesicular-arbuscular mycorrhiza formation in disturbed and undisturbed forest soils of southwest Oregon. Can. J. For. Res. 13:657-665.

Penman, J. L.. 1948. Natural evaporation from open water, bare soil and grass. Proc. Roy. Soc. London. A193:120-145.

Priestley C. H. B. and R. J. Taylor, 1972. On the assessment of surface heat flux and evaporation using large-scale parameters. Monthly Weather Review. 100(2):81-92.

Riha. S. J., K. J. McInnes, S. W. Childs, and G. S. Campbell. 1980. A finite element calculation for determining thermal conductivity. Soil Sci. Soc. Am. J. 44:1323-1325

Shuttleworth, W. J. and I. R. Calder. 1979. Has the Priestley-Taylor equation any relevance to forest evaporation? Journal of Applied Meteorology. 18:639-646.

Solmet Vol. 2. (1979). Hourly solar radiation-surface meteorological observations. Final Report TD-9724. National Climatic Center, Asheville, North Carolina.

Sorensen, F. C. and R. K. Campbell. 1978. Comparative roles of soil and air temperatures in the timing of spring bud flush in seedling Douglas-fir. Can. J. Bot. 56:2307-2308

Stevens, M. D. 1977. Standard distributions of clear sky radiance. Quart. J. Roy. Meteor. Soc., 103:457-465.

Stewart, R. B., 1983. A discussion of the relationships between the principal forms of the combination equation for estimating crop evaporation. Agric. Meteorol., 30:111-127.

Stewart, R. B. and W. R. Rouse, 1977. Substantiation of the Priestley and Taylor parameter α=1.26 for potential evaporation in high latitudes. Journal of Applied Meteorolgy. 16:649-650.

Tanner C. B. and W. A. Jury. 1976. Estimating evaporation and transpiration from a row crop during incomplete cover. Agronomy Journal. 68:239-243.

U.S.N.O. United States Naval Observatory; 1986. The Astronomical Almanac, U. S. Government Printing Office, Washington D. D..

van den Driessche, R. 1984. Response of Douglas fir seedlings to phosphorus fertilization and influence of temperature on this response. Plant and Soil 80:155-169.

Weiss, A. and Norman, J.M. 1984. Partitioning solar radiation into direct and diffuse, visible and near-infrared components. Agric. For. Meteorol., 34:205-213.